

1 **An integrated approach to determine interactive genotoxic and global gene**
2 **expression effects of multiwalled carbon nanotubes (MWCNTs) and**
3 **Benzo[a]pyrene (BaP) on marine mussels: Evidence of reverse ‘Trojan Horse’**
4 **effects**

5 Audrey Barranger^{a†}, Graham A. Rance^{b,c}, Yann Aminot^d, Lorna J. Dallas^a, Susanna Sforzini^e,
6 Nicola J. Weston^c, Rhys W. Lodge^{b,c}, Mohamed Banni^{e,f}, Volker M. Arlt^{g,h}, Michael N. Moore^{a,i,j},
7 James W. Readman^{d,i}, Aldo Viarengo^e, Andrei N. Khlobystov^{b,c}, Awadhesh N. Jha^{a*}

8 ^a*School of Biological and Marine Sciences, University of Plymouth, PL4 8AA Plymouth, United Kingdom;*

9 ^b*School of Chemistry, University of Nottingham, University Park, NG7 2RD Nottingham, UK;* ^c*Nanoscale*

10 *and Microscale Research Centre, University of Nottingham, NG7 2RD Nottingham, UK;* ^d*Centre for*

11 *Chemical Sciences, University of Plymouth, PL4 8AA Plymouth, United Kingdom;* ^e*Ecotoxicology and*

12 *Environmental Safety Unit, Istituto di Ricerche Farmacologiche Mario Negri IRCCS, Via Giuseppe La*

13 *Masa 19, 20156 Milan, Italy;* ^f*Laboratory of Biochemistry and Environmental Toxicology, ISA*

14 *chottMariem, Sousse University, Sousse, Tunisia;* ^g*Department of Analytical, Environmental and*

15 *Forensic Sciences, King’s College London, MRC-PHE Centre for Environmental & Health, SE1 9NH*

16 *London, United Kingdom;* ^h*NIHR Health Protection Research Unit in Health Impact of Environmental*

17 *Hazards at King’s College London in partnership with Public Health England and Imperial College*

18 *London, SE1 9NH London, United Kingdom;* ⁱ*Plymouth Marine Laboratory, Prospect Place, The Hoe, PL1*

19 *3HD Plymouth, United Kingdom;* ^j*European Centre for Environment & Human Health (ECEHH),*

20 *University of Exeter Medical School, Knowledge Spa, Royal Cornwall Hospital, TR1 3LJ Truro, Cornwall,*

21 *United Kingdom*

22 **Running Title:** *Interactive effects of multiwalled carbon nanotubes (MWCNTs) and Benzo[a] pyrene*
23 *(BaP) on marine mussels*

24 *Correspondence: Awadhesh N. Jha, School of Biological and Marine Sciences, University of Plymouth,
25 Plymouth, PL4 8AA, UK. E-mail: a.jha@plymouth.ac.uk/

26

27 [†]Present address: Université de Rennes 1 / Centre National de la Recherche Scientifique, UMR 6553

28 ECOBIO, Rennes, F-35000, France

29 **An integrated approach to determine interactive genotoxic and global gene expression**
30 **effects of multiwalled carbon nanotubes (MWCNTs) and Benzo[a] pyrene (BaP) on marine**
31 **mussels: Evidence of reverse ‘Trojan Horse’ effects**

32 **Abstract**

33 The interactions between carbon-based engineered nanoparticles (ENPs) and organic pollutants
34 might enhance the uptake of contaminants into biota. The present integrated study aimed to
35 assess this potential ‘Trojan Horse’, probing the interactive effects of purpose-made multi-
36 walled carbon nanotubes (MWCNTs), a representative ENP, and benzo[a]pyrene (BaP), a
37 ubiquitous polycyclic aromatic hydrocarbon (PAH) pollutant, on the marine mussel *Mytilus*
38 *galloprovincialis*. Mussels were exposed to MWCNTs and BaP either alone or in various
39 combinations. The co-exposure of BaP with MWCNTs revealed that the presence of MWCNTs
40 enhanced the aqueous concentrations of BaP, thereby reducing the uptake of this pollutant by
41 mussels as evidenced by lowering BaP concentrations in the tissues. Determination of DNA
42 damage (comet assay) showed a concentration- dependent response for BaP alone which was
43 absent when MWCNTs were present. Global gene expression using microarray analyses
44 indicated that BaP and MWCNTs, in combination, differentially activated those genes which are
45 involved in DNA metabolism compared to the exposures of BaP or MWCNTs alone, and the gene
46 expression response was tissue-specific. Mechanisms to explain these results are discussed and
47 relate primarily to the adsorption of BaP on MWCNTs, mediated potentially by van der Waals
48 interactions. The use of a novel approach based on gold-labelled MWCNTs to track their uptake
49 in tissues improved the traceability of nanotubes in biological samples. Overall, our results did
50 not indicate the ‘Trojan Horse’ effects following co-exposure to the contaminants and clearly
51 showed that the adsorption of BaP to MWCNTs modified the uptake of the pollutant in marine
52 mussels.

53 **Keywords:** *Mytilus galloprovincialis*; benzo[a]pyrene; multi-walled carbon nanotubes; van der
54 Waals interactions; adsorption

55

56 Introduction

57 The production of manufactured or engineered nanoparticles (ENPs) and nanomaterials (NMs) has
58 grown extensively over the last few years and they are entering into the environment (Giese *et al.*,
59 2018). Both academic and industrial researchers are extensively exploring their unusual, size-
60 dependent properties to develop the next generation of functional materials. The research effort has
61 led to the exploration of a number of promising applications of ENPs and NMs, particularly in the
62 health sector, where their potential utilisation as targeted drug delivery agents are being investigated
63 (Cho *et al.* 2008). However, to date most of the actual applications of ENPs and NMs are associated
64 with consumer products, e.g. in cosmetics, food and food packaging, paints and coatings (Foss Hansen
65 *et al.* 2016). In fact, in January 2019, it was reported that more than 3,000 products in Europe alone
66 contained NPs and NMs, with the database having grown by 1,000 products over the course of just 18
67 months (Foss Hansen *et al.* 2016; <http://nanodb.dk/>). Yet, whilst the benefits and improvements
68 offered by nanotechnology are well established, significant concern regarding the potential risks have
69 been raised. This stems from the fact that nanoscale materials, in common with other pollutants, can
70 enter the aquatic environment through different routes (Giese *et al.*, 2018) with very little research to
71 assess their potential impact on human health and the natural environment established.

72 Among ENPs, carbon-based nanoparticles, especially carbon nanotubes (CNTs), are of major
73 commercial interest, currently incorporated in a diverse range of commercial products, from
74 rechargeable batteries and automotive parts to sporting goods and in water filters (DeVolder *et al.*
75 2013). CNTs have the highest production volumes among engineered carbonaceous nanomaterials
76 worldwide (Gottschalk *et al.* 2013), exceeding 730 tonnes per year in Europe (Sun *et al.* 2016). Based
77 on this production data, the latest predictions estimate the environmental concentrations of CNTs in
78 surface water at 0.28 ng L^{-1} ($Q_{0.15} = 0.04 \text{ ng L}^{-1}$; $Q_{0.85} = 0.65 \text{ ng L}^{-1}$) (Sun *et al.* 2016). With a substantial
79 rise in the production and use of CNTs expected over the coming years, the concentrations of CNTs in
80 all environmental compartments, including the aquatic environment, will inevitably increase. Of
81 particular concern are multi-walled carbon nanotubes (MWCNTs) as they are presently used to reduce
82 the biofouling of ship hulls by discouraging the attachment of algae and barnacles (Beigbeder *et al.*
83 2008) and hence are directly released into the marine environment.

84 Whilst the presence of nanoscale materials in seawater represents a significant current issue, it is, in
85 fact, their potential combination with other ubiquitous contaminants that represents a far more
86 pressing concern. Carbon nanotubes, possessing a large hydrophobic surface area, have a high
87 adsorption capacity for hydrophobic molecules and thus a high affinity for co-released environmental
88 pollutants. Among these contaminants, polycyclic aromatic hydrocarbons (PAHs) represent a
89 significant concern. One of them, benzo[*a*]pyrene (BaP), is a known mutagenic and carcinogenic
90 contaminant, present in human foods as well as being ubiquitous in environmental samples
91 (Sogbanmu *et al.* 2016, Acevedo-Whitehouse *et al.* 2018; Di *et al.*, 2011). It is on the list of the priority
92 pollutants of the European Water Framework Directive (2000/60/CE) and is also a monitored PAH of
93 the United States Environmental Protection Agency (USEPA). To date, few studies have investigated
94 the interactive effects of carbon-based nanoparticles with different environmental pollutants on
95 aquatic organisms, especially marine organisms, with significant inconsistencies in the results
96 reported (reviewed in Canesi *et al.* 2015; Barranger *et al.*, 2019). Indeed, available data on the
97 combined effects of CNTs and other contaminants in aquatic organisms are inconclusive, if not
98 conflicting. Some studies indicate that the adsorption of pollutants to CNTs reduces their
99 bioaccumulation in organisms (Ferguson *et al.* 2008), whereas others highlight that co-exposure with

100 CNTs may amplify the toxic effects of other compounds by increasing their cellular uptake and
101 accumulation (Sun *et al.* 2014). These conflicting results could be explained by current evidence
102 suggesting that the variability in bioavailability of CNT-adsorbed organic contaminants is largely driven
103 by the size, configuration and surface area coverage of the contaminant on the nanomaterial (Linard
104 *et al.* 2017).

105 In addition to conflicting genotoxicological studies, one of the major challenges that has limited the
106 investigation of CNT uptake in environmental studies is the lack of a method to quantify them in
107 biological or environmental media. A recent review (Bjorkland *et al.* 2017) highlighted that CNTs have
108 been detected in environmental matrices and organisms using a broad range of analytical techniques,
109 including optical spectroscopies, electron microscopy, thermal methods and radiolabelling. However,
110 these methods are generally qualitative or at best quantitative with some bias and do not precisely
111 determine the concentration of CNTs in organisms.

112 With knowledge of the above information, in this study, we evaluated the interactions between
113 MWCNTs and the ubiquitous environmental pollutant BaP on marine mussels. Firstly, we analysed the
114 aggregation properties and genotoxicity of MWCNTs using light scattering and two different assays
115 (the comet and the micronucleus assays), respectively. Secondly, in a series of experiments where
116 mussels were co-exposed to MWCNTs and BaP at different concentrations, we measured the uptake,
117 expression of genes related to DNA metabolism as well as DNA damage and bulky DNA adduct
118 formation in mussels. Finally, we probed the novel application of gold-labelled MWCNTs as a method
119 to improve the tracking of carbon nanotubes in mussel tissues, utilising both spectroscopy and
120 electron microscopy approaches. This integrated and interdisciplinary strategy allowed us to test
121 whether the combination of BaP with MWCNTs induces molecular pathways different to those
122 observed for the pollutant alone and thus the viability of MWCNTs as a potential 'Trojan Horse' effects.

123 **Materials and Methods**

124 ***Mussel collection and maintenance***

125 Mussels (*Mytilus galloprovincialis*; 45-50 mm) collected from the intertidal zone at Trebarwith Strand,
126 Cornwall, a reference site (50° 38' 40" N, 4° 45' 44" W) were maintained under laboratory conditions
127 prior to experimentations as described previously (Dallas *et al.* 2013, D'Agata *et al.* 2014, Vernon and
128 Jha 2019).

129 ***Preparation and characterisation of MWCNTs***

130 MWCNTs were purchased from NanoLab, USA (PD30L520, synthesised by chemical vapour
131 deposition). In the absence of a single Organisation for Economic Cooperation and Development
132 (OECD) standard for MWCNTs (OECD Environmental, Health and Safety Publications Dossier No. 68),
133 these MWCNTs were selected owing to their structural and physicochemical similarities to other
134 MWCNTs commonly reported in the wider literature. Moreover, the study of MWCNTs, rather than
135 single-walled carbon nanotubes (SWCNTs), was deemed more imperative given their greater
136 commercial application and thus propensity to be released into the natural environment. To
137 homogenise the nanotube length distribution, MWCNTs were shortened and purified using a multi-
138 step strategy based on site-selective catalytic oxidation (LaTorre *et al.* 2010, Miners *et al.* 2014). In

139 studies on bivalve molluscs, ENPs and NMs are typically characterised in seawater without animals
140 (Gomes *et al.* 2013, D'Agata *et al.* 2014), which is not strictly speaking representative of the
141 experimental conditions. In order to better replicate the conditions of the experiment during analysis,
142 mussels (4.5 mussels L⁻¹) were maintained in 2-L glass beakers for 24 h with natural seawater from
143 Plymouth Sound (filtered at 10 µm). Subsequently, MWCNTs (1 mg) were added to the mussel-
144 exposed seawater (10 mL) and the suspension homogenised by ultrasonication (Langford Sonomatic
145 375, 40 kHz) for 1 h at room temperature. The suspension was allowed to settle for at least 4 h at
146 room temperature prior to analysis of the aggregate size. Control measurements of aggregate size in
147 (i) seawater, in the absence of mussels and (ii) mussel-exposed seawater in the presence of BaP (1 mg
148 L⁻¹) were additionally performed. Dynamic light scattering (DLS) was performed using a Malvern
149 Zetasizer Nano-ZS at room temperature. Quoted values are the average of 2-3 measurements. Bright
150 field transmission electron microscopy (TEM) was performed using the JOEL 2100+ microscope
151 operated at 200 keV. Energy dispersive X-ray (EDX) spectra were acquired using an Oxford Instruments
152 INCA X-ray microanalysis system and processed using Aztec software. Samples were prepared by
153 casting several drops of the respective suspensions onto copper grid-mounted lacey carbon films.

154 ***Exposure of Mytilus galloprovincialis to MWCNTs***

155 ***Experimental design***

156 After depuration, the mussels were transferred to 2-L glass beakers containing 1.8 L of the same
157 seawater as above and allowed to acclimatise for 48 h. Two mussels were used per beaker. A
158 photoperiod of 12 h light, 12 h dark was maintained throughout the experiment. Good seawater
159 oxygenation was provided by a bubbling system. The seawater quality was monitored in each of the
160 beakers by measuring the salinity (36.65 ± 0.18‰), pH (7.98 ± 0.04), percentage of dissolved oxygen
161 (97.09 ± 1.28%) and temperature (14.89 ± 0.13°C). Mussels were exposed to different treatments for
162 7 days: a seawater control (12 mussels); a positive control (0.04 mg L⁻¹ CuSO₄; 12 mussels); 0.01 mg L⁻¹
163 MWCNTs (12 mussels); 0.1 mg L⁻¹ MWCNTs (12 mussels); and 1 mg L⁻¹ MWCNTs (12 mussels).
164 MWCNTs were pre-weighed in glass vials for each beaker according to the required final concentration
165 (0.018 mg, 0.18 mg and 1.8 mg to reach 0.01, 0.1 and 1 mg L⁻¹ respectively) and directly tipped in the
166 beakers. Mussels were not fed and did not spawn during the experiment. At the end of the exposure,
167 10 mussels were sampled for each treatment. Two different tissues, gills and digestive gland (DG) were
168 used to perform the comet assay and the micronucleus assay. Gill and digestive gland cells were
169 chosen to unravel the potential interactive toxic effects of MWCNTs and BaP. In mussels, feed particles
170 are filtrated first through gills and transported up to the digestive gland (DG) to be metabolized. This
171 leads to high bioaccumulation of contaminants in this tissue. It is to be noted that as an analogue to
172 mammalian liver, enzymes involved in the biotransformation of both endogenous and exogenous
173 substrates are mainly localized in the digestive gland of mussels (Livingstone and Pipe 1992, Akcha *et al.*
174 *al.* 1999).

175 ***Comet assay to determine DNA damage***

176 The comet assay on gill and digestive gland (DG) cells (n = 10) was performed as previously described
177 by us (Dallas *et al.* 2013, Banni *et al.* 2017, Vernon and Jha 2019).

178 **Micronucleus assay**

179 For the micronucleus assay, tissues (i.e. gill and DG) were digested with the same protocol as for the
180 comet assay. The cell suspension was spread gently across the slide with a clean cover slip, allowed to
181 adhere onto the slides by placing in the fridge for 1 h. To fix the cells, the dried slides were immersed
182 in a coupling jar containing Carnoy's fixative for 20 min. Following fixation, the slides were stained
183 with 20µl of ethidium bromide (20 µg mL⁻¹). Slides were randomised and scored under the microscope
184 for the induction of micronuclei. At least 1000 cells were scored from each slide (two slides per
185 individual mussel) according to the detailed criteria described elsewhere (Bolognesi and Fenech 2012,
186 Dallas *et al.* 2013, Vernon and Jha 2019).

187 **Exposure of *Mytilus galloprovincialis* to BaP and MWCNTs**

188 **Experimental design**

189 In a separate experiment, mussels were exposed for 3 days (with no water changes) to BaP alone (5,
190 50 and 100 µg L⁻¹), MWCNTs alone (1 mg L⁻¹) and a combination of BaP and MWCNTs (1 mg L⁻¹ MWCNTs
191 + 5 µg L⁻¹ BaP; 1 mg L⁻¹ MWCNTs + 50 µg L⁻¹ BaP; 1 mg L⁻¹ MWCNTs + 100 µg L⁻¹ BaP). Concurrently,
192 mussels were also exposed to a solvent control (0.02% DMSO). Due to the chemical composition of
193 seawater, the occurrence of PAHs (very hydrophobic compounds), is at very low levels (<1 ng/L), in
194 contrast to concentration in other aqueous matrices. For example, in marine sediments, the
195 corresponding values could be in the range of 1 ng/g d.w. to >10000 ng/g d.w. (Nikolaou *et al.* 2009).
196 In marine mussels, depending on the study area, PAHs can be found at concentrations ranging from
197 25 to 3 900 ng/g d.w. (Baumard *et al.* 1998, 1999), corresponding to our lowest exposure
198 concentration (5µg.L⁻¹). Regarding the selection of higher BaP exposure concentrations (50 and 100
199 µg.L⁻¹), previous studies have reported that the selected concentration-range induced biological or
200 biomarker responses in mussels (Halldórsson *et al.* 2008, Di *et al.* 2011, Banni *et al.* 2017). In the
201 present study, for each treatment, 26 mussels were used. As previously described, MWCNTs were pre-
202 weighed in glass vials for each beaker according to the final concentration (1.8 mg to reach 1 mg L⁻¹)
203 and directly tipped into the beakers. Seawater quality was monitored in each of the beakers by
204 measuring the salinity (36.42 ± 0.05‰), pH (7.72 ± 0.11), percentage of dissolved oxygen (94.58 ±
205 2.40%) and temperature (15.55 ± 0.32°C).

206 **Chemical analysis of BaP in water and tissue**

207 Water and tissue extracts were analysed using an Agilent Technologies (Stockport, UK) 7890A Gas
208 Chromatography (GC) system interfaced with an Agilent 5975 series Mass Selective (MS) detector as
209 described previously by us (Banni *et al.* 2017).

210 **DNA metabolism gene expression**

211 **Microarray hybridisation and analysis.** Competitive dual-colour microarray hybridisation was
212 performed with the STREM (Stress Response Microarray in *Mytilus sp.*) platform (Banni *et al.* 2017);
213 fluorescence-labelled cDNA probes were obtained by direct labelling in the presence of modified Cy3-
214 and Cy5-dCTP (Perkin Elmer). The procedure was carried out as described previously (Banni *et al.* 2011,
215 2017). MIAMI-compliant microarray data, including a detailed description of the experimental design

216 and each hybridization experiment, were deposited in the Gene Expression Omnibus
217 (<http://www.ncbi.nlm.nih.gov/geo/query/>).

218 **Functional genomics analysis**

219 Functional characterisation of mussel genes represented on a microarray was based on Gene Ontology
220 (GO) annotation and carried out in Blast2GO (Conesa *et al.* 2005) using default parameters. However,
221 in the case of the STREM platform, target genes were putatively annotated and ranked under
222 established biological processes, making the generation of robust processes easier and faster.

223 *qRT-PCR*. qRT-PCR analysis was carried out using the same RNA extracted for microarray hybridization.
224 Relative mRNA abundance of the mussel genes encoding 4 Probes and primer pairs (Table S2) were
225 designed using Beacon Designer v3.0 (Premier Biosoft International, Inc.). The procedure is described
226 in (Banni *et al.* 2011, 2017).

227 **Comet assay**

228 The comet assay was performed as reported above (section “Comet assay to determine DNA
229 damage”) with gills and DG tissues from 10 mussels for each treatment.

230 **DNA adducts**

231 DNA from 10 mussels for each treatment was isolated from gills and DG tissues using a standard
232 phenol-chloroform extraction procedure. We used the nuclease P1 enrichment version of the thin-
233 layer chromatography (TLC) ³²P-postlabelling assay to detect BaP-derived DNA adducts (i.e. 10-
234 (deoxyguanosin-*N*²-yl)7,8,9-trihydroxy-7,8,9,10-tetrahydro-BaP [dG-*N*²-BPDE]). The procedure was
235 essentially performed as described previously (Phillips and Arlt 2014).

236 **Evaluation of the uptake of gold-labelled MWCNTs by mussels**

237 *Synthesis of labelled nanotubes*

238 To probe the uptake of carbon nanotubes by the mussels, it was necessary to label the nanotubes
239 with a diagnostic marker. Gold was selected for this purpose due to its relatively low abundance in the
240 natural environment (Goldberg 1987), thus providing an excellent spectroscopic handle facilitating
241 ease of detection by both bulk and local-probe spectroscopy approaches. Confinement of
242 nanoparticles within the internal void of MWCNTs is a highly efficient process allowing retention of
243 the metal label in the system (Miners *et al.* 2016) and simultaneously excluding any interference of
244 the label with measurements on nanotubes. Gold nanoparticles were synthesised using a modified
245 Brust-Schiffrin reduction (Rance *et al.* 2008) followed by insertion into MWCNTs utilising a thermally-
246 assisted Ostwald ripening procedure yielding AuNP@MWCNTs (Scheme S1).

247 **Experimental design**

248 Mussels were exposed to labelled MWCNTs only (1 mg L⁻¹ AuNP@MWCNTs) and in combination with

249 BaP as the same concentration as above (1 mg L⁻¹ AuNP@MWCNTs + 5 µg L⁻¹ BaP; 1 mg L⁻¹
250 AuNP@MWCNTs + 50 µg L⁻¹ BaP; 1 mg L⁻¹ AuNP@MWCNTs + 100 µg L⁻¹ BaP). Four mussels were used
251 for each treatment.

252 ***Bulk spectroscopic analysis***

253 For the determination of tissue-specific gold concentration, 4 mussels per treatment were analysed
254 by inductively coupled plasma mass spectrometry (ICP-MS). Each individually dissected tissue (gills,
255 DG, all other tissues pooled together) was washed with distilled water, blotted dry and transferred to
256 a pre-weighed acid washed vial. Samples were dried overnight at 60°C and re-weighed. Tissue
257 digestion was achieved by addition of 1 mL concentrated nitric acid (trace analysis grade) and
258 incubation for 2 h at 70°C. Digested tissue samples were diluted to a final volume of 5 mL with
259 Millipore Milli Q water and stored at room temperature until analysis. An internal standard of 115-In
260 was added, to a final concentration of 10 µg L⁻¹. This verified that instrumental drift was not the cause
261 of sample variation. Indium was selected based on its minimal occurrence in marine samples and low
262 polyatomic interference with seawater. Samples were analysed using an X Series II ICP-MS (Thermo
263 Fisher Scientific Inc., Waltham, MA, USA) with PlasmaLab software (Thermo Fisher Scientific Inc.,
264 Waltham, MA, USA).

265 ***Mussel sectioning and electron microscopy analysis***

266 To probe the spatial location of the labelled MWCNTs with respect to the mussel DG, samples of whole
267 tissues and cross-sections were analysed by environmental scanning electron microscopy (ESEM) and
268 scanning transmission electron microscopy (STEM), respectively. In either case, after the exposure
269 experiments detailed above, a small piece (~5 mm²) was dissected out of the centre of the digestive
270 gland and fixed in 2% paraformaldehyde, 2.5% glutaraldehyde, 2.5% NaCl, 2 mM CaCl₂ in 0.1 M PIPES,
271 pH 7.2 for 3 h. The tissue was then stored in 2.3 M sucrose (in 0.1 M PIPES) until analysis. Two mussels
272 were analysed per treatment. Whole tissue samples were washed with deionised water (four times),
273 transferred onto aluminium specimen stubs and imaged at 3°C (cooled using the Peltier stage) in ESEM
274 mode with the backscatter detector using the FEI Quanta 650 ESEM. Electron transparent sections for
275 STEM analysis were prepared by cutting ~1 mm² pieces from the washed whole tissues and sectioning
276 to a thickness of ~180-200 nm at -80°C using the RMC Products PowerTome with the CR-X
277 cryochamber. The cross-sections were transferred onto copper-grid mounted graphene oxide films
278 using the Tokuyasu technique and imaged in dark field STEM using the JOEL 2100+ microscope
279 operating at 200 keV.

280 ***Statistical analyses***

281 Statistical tests were conducted using R software. Normality was checked using Lilliefors's test and
282 variance homogeneity was evaluated using Bartlett's test. When necessary, raw data were
283 mathematically transformed (Ln) to achieve normality before proceeding with an ANOVA. When
284 significant, a posteriori Tukey test was performed.

285 **Analysis of interactions**

286 The non-parametric Mann-Whitney *U*-test was used to compare the data from treated mussels with
287 those of the controls (Sforzini *et al.* 2018a). Further analysis of the combined effects of MWCNTs and
288 BaP on DNA Damage (based on Comet Assay) was performed by calculating the Interaction Factor (IF)
289 in order to test for evidence of additivity, synergism and antagonism (Schlesinger *et al.* 1992, Katsifis
290 *et al.* 1996, David *et al.* 2016; Zhang *et al.* 2019):

$$\begin{aligned} 291 \quad IF &= (G_{(MWCNT + BaP)} - C) - [(G_{(MWCNT)} - C) + (G_{(BaP)} - C)] \\ 292 \quad &= G_{(MWCNT + BaP)} - G_{(MWCNT)} - G_{(BaP)} + C \end{aligned} \quad (\text{Equation 1})$$

$$293 \quad SEM_{(IF)} = \sqrt{SEM^2_{(MWCNT + BaP)} + SEM^2_{(MWCNT)} + SEM^2_{(BaP)} + SEM^2_{(C)}} \quad (\text{Equation 2})$$

294 Where IF is the interaction factor: negative IF denotes antagonism, positive IF denotes synergism, and
295 zero IF denotes additivity. *G* is the mean cell pathological reaction to toxicants (BaP, MWCNTs and BaP
296 + MWCNTs), *C* is the mean cellular response under control conditions. *SEM*(*x*) is the standard error of
297 the mean for group *X*. Results were expressed as IF, and the 95% confidence limits were derived from
298 the SEM values.

299 In order to test the mixture IF values against predicted additive values (assumed to have an IF = 0),
300 the predicted additive mean values (*A*) were calculated:

$$301 \quad A = (G_{(MWCNT)} - C) + (G_{(BaP)} - C) \quad (\text{Equation 3})$$

302 The Pythagorean theorem method for combining standard errors was used to derive combined
303 standard errors for the predicted mean additive values (*A*) of MWCNTs and BaP
304 (<http://mathbench.org.au/statistical-tests/testing-differences-with-the-t-test/6-combining-sds-for-fun-and-profit/>). The standard errors for the three C60 and BaP treatments (predicted additive) were
305 derived using the following equation:
306

$$307 \quad SEM_{(add)} = \sqrt{SEM^2_{(MWCNT)} + SEM^2_{(BaP)} + SEM^2_{(C)}} \quad (\text{Equation 4})$$

308 This enabled the 95% confidence limits to be derived for the predicted additive values. The confidence
309 limits were used to test the predicted additive values having an IF = 0 against the IF values for the
310 mixtures.

311 **Results**

312 **Preparation and characterisation of MWCNTs in seawater**

313 Light scattering and electron microscopy analyses of MWCNTs, shortened and purified by the site-
314 selective, silver-catalysed nanotube oxidation procedure developed previously (Miners *et al.* 2014)
315 which yielded nanotubes ~600 nm in length (Figure 1b), in mussel-exposed seawater indicated the
316 formation of micron-sized aggregates (Figure 1c; S1 and S2). The mean aggregate size determined by
317 DLS (1541±193 nm) showed minimal variation relative to those measured in seawater in the absence

318 of mussels (1666±198 nm) and in the presence of BaP in mussel-exposed seawater (1642±431 nm).
319 [Figure 1]

320 ***Genotoxicity of MWCNTs in gill and digestive gland cells***

321 At the end of the exposure period, a subtle increase in DNA strand breaks was observed in both the
322 gills and the DG of mussels exposed to the highest concentrations of MWCNTs (0.1 and 1 mg L⁻¹)
323 relative to the seawater-only control (Figure 2). No effect was noted at the lowest concentration (0.01
324 mg L⁻¹). Furthermore, no increase in micronuclei was observed after MWCNTs exposure in the gills and
325 DG

326 [Figures 2 and 3]

327 ***Co-exposure to BaP and MWCNTs***

328 *BaP seawater concentration and uptake in mussel DG*

329 At one hour after dosing, the BaP concentrations in seawater were very close to the nominal
330 concentrations of 64, 81 and 129% for the 5, 50 and 100 µg L⁻¹ BaP-only exposures and 48, 78 and
331 113% for the co-exposures to MWCNT + BaP 5, 50 and 100 µg L⁻¹, respectively. At the end of the
332 exposure, a strong decrease was observed to approximately 95 and 85% of the initial value for
333 exposure to BaP alone and the co-exposure, respectively (Table S1).

334 As expected, the concentration of BaP in DG in the solvent and MWCNT-only control treatments was
335 below the limit of detection and found to increase with concentration in both the single and co-
336 exposure experiments. However, BaP uptake was significantly lower in mussels co-exposed to
337 MWCNTs and BaP (p<0.05), with a 78 and 44% decrease in the uptake for mussels exposed to MWCNTs
338 and BaP at concentrations of 50 and 100 µg L⁻¹, respectively, compared to mussels exposed to BaP
339 alone at the same concentrations (Table 1).

340 [Table 1 near here]

341 ***DNA metabolism gene expression***

342 The transcriptomic approach performed in this work is based on a new platform developed by our
343 group to investigate gene expression profiling of *Mytilus sp.* to environmental stressors. DNA
344 metabolism was the main investigated process over the 15 processes present on the array. Our data
345 revealed that over the 36 targets present on the array covering the DNA metabolism process, 27 were
346 involved in the response to BaP and MWCNTs in DG and 24 in the gills, in at least one condition. In DG,
347 the number of differentially expressed genes (DEGs) involved in the stress response was maximal at 5
348 µg L⁻¹ BaP and 100 µg L⁻¹ BaP with 14 DEGs and 12 DEGs respectively (Table 2). However, in the gills
349 the highest number of DEGs was observed in mussels exposed to BaP at 5 µg L⁻¹ and 100 µg L⁻¹ in the
350 presence of nanotubes (14 DEGs) providing the first clues about the distinct response to stress in the
351 two organs. The heat map clearly showed distinct pattern of DEGs in both tissues (Figures 4, Additional
352 information in Tables S3 and S4). In particular, p53, caspase 3, p63/73 and alkaline phosphatase

353 targets were found to be the most present in all conditions in the DG and gill tissues showing a distinct
354 pattern between conditions. Indeed, while, the maximum p53 expression level in digestive gland (M
355 value 1.88) was observed in mussels exposed to 5 $\mu\text{g L}^{-1}$ BaP, it was maximum in gills (M value 2.21)
356 for mussels exposed to nanotubes alone. Moreover, caspase 3 gene expression was maintained down
357 regulated in digestive gland tissues exposed to 5 $\mu\text{g L}^{-1}$ BaP (Mvalue -2.30) and nanotubes (M value -
358 3.08). However, the same target was observed to reach a maximum up-regulated level in digestive
359 gland tissues for mussels exposed to MWCNTs and BaP at concentrations of 50-100 $\mu\text{g L}^{-1}$ (M value
360 2.29). A similar trend was observed in gills. Gene expression analysis by qPCR of selected targets (e.g.
361 p53, caspase3, DNA ligase and topoisomerase) in the same tissues were in trend with the array data
362 (Figure S4).

363 [Table 2 and Figure 4]

364 ***DNA damage in gills and digestive gland after co-exposure***

365 Regarding the comet assay, a tissue-specific response was observed, the DG being more prone to DNA
366 damage compared to the gills. In DG, BaP-induced genotoxicity was concentration-dependent
367 whereas BaP+MWCNTs co-exposure reduced the genotoxic effects. As observed in the previous
368 experiment, exposure to MWCNTs induced DNA strand breaks. In the gills, BaP was only genotoxic at
369 the highest concentration 100 $\mu\text{g L}^{-1}$, and the co-exposure induced DNA damage only at the
370 intermediate concentration (Figure 5). No significant effect was observed in mussels exposed to
371 MWCNT only. No bulky BaP-DNA adducts (i.e. dG- N^2 -BPDE) were detected in any tissue at any of the
372 treatment condition (data not shown).

373 [Figure 5]

374 *Interactions.* Interactions between MWCNTs and BaP on DNA damage are shown in Table 3. There was
375 evidence of an antagonistic interaction between MWCNTs and BaP for DNA damage (Comet assay) at
376 the 5 and 100 $\mu\text{g L}^{-1}$ BaP + MWCNT combination treatment (Table 3).

377 ***Analysis of MWCNT uptake in mussels***

378 The presence of gold in the mussel tissues (from the DG, gills and all other tissues pooled together),
379 as diagnostic of the uptake of labelled MWCNTs, was quantified using ICP-MS. The highest amount of
380 gold was found in DG with a mean concentration of 66.73 $\mu\text{g g}^{-1}$ determined, approximately one order
381 of magnitude higher than that observed in the gills (9.42 $\mu\text{g g}^{-1}$) and all other tissues (5.52 $\mu\text{g g}^{-1}$). No
382 significant difference was observed in gold level between the different treatments (with or without
383 BaP) in all of the tissues (Figure 6). However, despite an exhaustive electron microscopy investigation
384 of whole and cross-sectioned DG tissues, no direct visualisation of nanotubes was afforded (Figures
385 S5-8).

386 [Figure 6]

387 Discussion

388 ***Characterisation of MWCNTs in relevant environmental media***

389 The size, shape and surface chemistry of nanoscale materials is known to affect their dispersion in
390 environmental media (Gottschalk *et al.*, 2013). Effective understanding of these physicochemical
391 parameters is key to their potential uptake and consequent biological impact on the marine biota. For
392 carbon-based nanoparticles, such as MWCNTs, this is particularly critical as their surfaces are
393 inherently hydrophobic. MWCNTs therefore have a strong tendency to form aggregates in water, the
394 size and stability of which depends on the properties of both the nanotube and the specific aqueous
395 environment. Indeed, our light scattering measurements (Figure S1) confirm the formation of stable
396 micron-sized agglomerates of nanotubes in mussel-exposed seawater, consistent with analogous
397 studies of MWCNT aggregates in both natural (Anisimova *et al.* 2015) and synthetic seawaters (Xu *et*
398 *al.* 2011, Cerrillo *et al.* 2015). Interestingly, there was no significant difference in the mean MWCNT
399 aggregate size observed in the mussel-exposed seawater, relative to nanotube aggregates formed in
400 seawater in the absence of mussels or mussel-exposed seawater in the presence of BaP. This suggests
401 that enhancing the propensity for interactions of MWCNTs with either the proteins secreted by
402 mussels or small aromatic molecules does not, in these instances, aid the solvation of individual
403 MWCNTs or affect the observed aggregate sizes formed in seawater. This is however not expected to
404 be a general phenomenon. We therefore recommend that all future ecotoxicological studies on ENPs
405 and NMs feature analysis in the species of interest to account for any possible effects of this nature.

406 ***Genotoxicity of MWCNTs***

407 Despite their environmental relevance, little information is available regarding the genotoxicity of
408 carbon nanoparticles and in particular carbon nanotubes in marine invertebrates. In our study, DNA
409 strand breaks were observed in mussel gills and DG after 7-days exposure to 0.10 and 1 mg L⁻¹ to
410 MWCNTs and in DG after 3-days exposure to 1 mg L⁻¹ MWCNTs. However, no effect was observed in
411 gills after 3-days exposure to 1 mg L⁻¹ MWCNTs suggesting a tissue specific genotoxic effect of
412 MWCNTs in mussels. In the marine polychaete *Arenicola marina*, no significant effect on DNA strand
413 breaks was observed after 10 days of exposure to single-walled carbon nanotubes (SWCNTs) through
414 natural sediment (0.003 and 0.03 g/kg) (Galloway *et al.* 2010). Regarding other carbon nanomaterials,
415 increased DNA strand break formation was observed in haemocytes of the marine mussels after
416 exposure to C₆₀ at 0.10 and 1 mg L⁻¹ for 3 days (Al-Subiai *et al.* 2012, Di *et al.* 2017).

417 The mechanism of genotoxicity of CNTs in bivalve cells remains unknown. Genotoxic responses of
418 CNTs may arise via direct mechanical injury or as a secondary result of CNT-mediated reactive oxygen
419 species (ROS) generation and therefore oxidative stress (Hutchison *et al.* 2010). Among these
420 mechanisms, oxidative stress is indicated as the key factor of genotoxicity induced by ENMs in bivalve
421 species and their accumulation associated with exposure time is also an important factor in induced-
422 genotoxicity (Rocha *et al.* 2015). Studies by De Marchi *et al.* (2017a, 2017b) in two polychaete species
423 (*Diopatra neapolitana* and *Hediste diversicolor*) and in a marine bivalve (*Ruditapes philippinarum*)
424 showed the induction of oxidative stress after 28 days of exposure to MWCNTs (0.10 and 1.00 mg L⁻¹
425 ¹). Elevated ROS levels may activate cellular stress-dependent signalling pathways. It can directly
426 damage mitochondria, cause DNA fragmentation in the nucleus, cell cycle arrest, apoptosis, and/or
427 inflammatory responses (Nel *et al.* 2006, Maurer-Jones *et al.* 2013). In mammalian cells, it has been

428 shown that CNTs are able to induce a range of different genotoxic effects. Among these damages,
429 CNTs can also impair the functionality of the mitotic apparatus inducing micronuclei and chromosomal
430 aberrations (VanBerlo *et al.* 2012). However, in our study, no potential aneugenic effect was studied
431 with the micronucleus assay due to lack of species specific centromeric probes. Currently, the
432 genotoxic potential of CNTs in marine invertebrates is not clear. Various factors could influence this
433 phenomenon including differences in experimental design among studies, experimental models used,
434 exposure routes, type of CNTs examined and their preparation procedures, concentrations used and
435 assessed endpoints.

436 **Co-exposure to BaP and MWCNTs**

437 The main objective of this study was to determine if a ‘Trojan Horse’ effect could be observed when
438 mussels were exposed to MWCNTs in combination with BaP. Mussels accumulated BaP in gills and DG
439 in a manner consistent with previous studies (Canova *et al.* 1998, Banni *et al.* 2017). It was however
440 interesting to observe a decrease in BaP uptake when mussels were co-exposed to MWCNTs. In the
441 Japanese Medaka (*Oryzias latipes*), it has been shown that the coexistence of SWCNTs facilitated the
442 accumulation of phenanthrene in the digestive track of fish and therefore enhanced the whole-body
443 phenanthrene concentration (Su *et al.* 2013). In the earthworm (*Eisenia foetida*), the addition of
444 nanotubes in soil significantly decreased pyrene uptake (Petersen *et al.* 2009b). The same
445 contradictory results were observed with other carbon nanoparticles as for example fullerenes. Della
446 Torre *et al.* (2017) demonstrated that carbon nanopowder facilitated BaP uptake by zebrafish embryos
447 and also affected the distribution of the pollutant in the organism. However, in the same species (i.e.
448 zebrafish larvae), it has been shown that bioavailability of 17 α -ethynylestradiol (EE2) was reduced
449 with increasing concentration of nC60 nanoparticles (Park *et al.* 2011). Interestingly, in the digestive
450 gland of *M. galloprovincialis*, comparable BaP tissue concentrations in the presence or absence of C₆₀
451 were observed indicating that, despite the expected strong sorption of BaP on C₆₀, no ‘Trojan horse’
452 effect was observed and C₆₀-sorbed B[a]P also remained bioavailable (Barranger *et al.* 2019). In our
453 study, this decrease in BaP uptake when mussels were co-exposed to MWCNTs could be due to high
454 adsorption properties of MWCNTs towards organic compounds and in our case BaP, as widely
455 described for carbon-based ENPs (Yang *et al.* 2006; Hu *et al.* 2008, 2014). Our results showed that BaP
456 is more present in the seawater and less in the DG at the end of the exposure period when MWCNTs
457 are present. Our results suggest that adsorption of BaP on MWCNTs through van der Waals
458 interactions (Figure 1a) in seawater prevent BaP from reaching the mussel. Genotoxic effects
459 measured by the Comet assay confirmed these results showing less DNA damage (i.e, antagonistic
460 interaction, Table 3) in DG when mussels are co-exposed to BaP and MWCNTs, as a result of a lower
461 bioavailability of BaP adsorbed on MWCNTs (Zhang *et al.* 2019). Previous studies demonstrated that
462 hydrophobic interactions largely drive adsorption of PAHs to MWCNTs (Linard *et al.* 2017).
463 Bioavailability appears to be more influenced by the ability of PAH molecules to access the available
464 adsorption sites, as a function of molecular size and morphology, rather than the type of carbon
465 nanomaterial (Xia *et al.* 2012, Linard *et al.* 2017).

466 MWCNTs are relatively large supra-molecular structures but may have limited access into the DG cells
467 by endocytosis (Maruyama *et al.* 2015). However, BaP will probably enter the DG cells through a
468 combination of direct transfer (Plant *et al.* 1985) and through endocytosis in bound form mediated by
469 Van der Waals interaction with food proteins and lipids; or else bound to cell surface proteins (Rashid
470 *et al.* 1991, Moore *et al.* 2004, Sayes *et al.* 2004). Most of the observed DNA damage will probably
471 result from oxidative injury to DNA by ROS generated from futile cycling of BaP; as well as being

472 produced by the MWCNTs and by intra-lysosomal lipofuscin associated with iron (Brunk and Terman
473 2002, Zangar *et al.* 2004, Moore *et al.* 2007, Sforzini, Moore, *et al.* 2018). The antagonistic interaction
474 observed for highest test concentration of MWCNT + BaP combinations probably result from the
475 consequences of an intracellular limitation of oxidative damage in the mixture treatment (DellaTorre
476 *et al.* 2018). Such limitation may be caused by binding of BaP to externalised non-endocytosed
477 MWCNTs resulting in reduced entry and bioavailability of BaP as evidenced by reduced BaP in DG
478 (Table 1), hence, reducing ROS generation.

479 In addition to this adsorption effect, according to the literature, various nanoparticles suspended in
480 seawater form aggregates of nano- and microsized (Canesi *et al.* 2010a, Canesi *et al.* 2010b, Canesi *et al.*
481 *et al.* 2014). In the presence of bivalves, the aggregates associate with mucus are suggested to be
482 deposited along the byssus thread and settle on the bottom of the aquarium (Canesi *et al.* 2010b).
483 Thus, the amount of nanoparticles, and in our case of BaP adsorbed on it, captured by mollusks is
484 significantly less than that expected on the basis of the initial concentration of the suspension. These
485 results could lead to the hypothesis that the high sedimentation rate observed within aquarium
486 highlighted that MWCNTs would transport PAHs mainly in sediments (DellaTorre *et al.* 2017, 2018).

487 Regarding other genotoxic effects, in our study no bulky BaP-DNA adducts were detected in any of the
488 treatments. This result differs with a previous experiment (Banni *et al.* 2017), where bulky DNA
489 adducts (i.e. dG-N²-BDDE) were detected after exposure to BaP using the same experimental design
490 (same concentrations and exposure duration). One explanation could be the physiological state of the
491 mussels. It is known that mussels from the species *Mytilus galloprovincialis*, are spawning all year
492 around compared to *Mytilus edulis* which has a specific period of spawning in May and October. Even
493 if we performed our experiment in November, gonads of mussels were mature, and it is known that
494 during maturation there is a drop in the biotransformation process that could explain the lack of bulky
495 BaP-DNA adducts in DG (Solé *et al.* 1995, Shaw *et al.* 2004).

496 In addition to the biomarkers of genotoxic effects, the transcriptomics data provided interesting
497 information regarding the expression of genes involved in DNA metabolism. We noticed a marked
498 regulation of genes involved in DNA metabolism in both tissues in mussels exposed to BaP alone or in
499 combination with MWCNTs. However, exposure to MWCNTs alone resulted in a very low number of
500 DEGs in both tissues. Interestingly, mussels exposed to the mixtures of BaP and nanotubes manifested
501 a significant increase in the number of DEGs in gills while no marked increase was observed in DG. In
502 the last decade, transcriptomics has proved to be a reliable tool, increasing our understanding of many
503 important physiological processes in marine organisms in response to environmental stressors such
504 as chemicals (Negri *et al.* 2013; Sforzini *et al.* 2018b) as well as to physiological parameters such as
505 annual cycle (Banni *et al.* 2011). Moreover, transcriptional control can allow stressed organisms to
506 cope with the alteration of cellular functions and to avoid cellular damage.

507 A significant alteration was recorded by the Comet assay in DG cells from animals exposed to BaP
508 alone, and co-exposed to BaP and MWCNTs but to lesser extent. Transcriptomic data corroborated
509 these results showing less DEGs in DG of mussels co-exposed to the mixture. In gills however mussels
510 exposed to the mixture of BaP and MWCNTs exhibited a significant increase in the number of DEGs.
511 These results are not correlated with the genotoxic response measured by Comet assay showing no
512 additional effect when mussels are co-exposed to both contaminants. The relatively short exposure
513 period (3 days) may explain the absence of cellular alterations where gene expression occurs.

514 The investigation of DNA damage response genes coding for caspase (HQ424451.1) revealed a marked

515 up-regulation of apoptotic genes in gills of mussels exposed to the highest BaP concentration alone or
516 in combination with nanotubes. DNA repair-related enzymes (DNA ligase: AJ624686.1; p53:
517 KC545827.1) were however markedly up-regulated in animals exposed to lower BaP concentration
518 and to nanotubes (data confirmed by qPCR). Mussel's cells may react to DNA alterations via p53-
519 mediated cell cycle arrest or apoptosis, upon high or irreparable DNA damage, p53 promotes the cells
520 towards apoptosis (Schwartz and Rotter 1998).

521 Overall, these results highlight that, once inside the organism, BaP and MWCNTs activate genes
522 involved in DNA metabolism in a different way to the activation by BaP or MWCNTs alone. Genotoxic
523 and transcriptomic data may suggest a tissue-specific response and the occurrence of a DNA repair or
524 apoptosis events with respect to the applied BaP/nanotubes concentrations. In our case, it is difficult
525 to conclude the exact mechanisms of this response. Despite the fact that less BaP is uptaken when
526 mussels are co-exposed, gills displayed higher DEGs in the co-exposure treatment, which is not the
527 case for DG. It has been shown that BaP accumulates differently in tissue when zebrafish embryos are
528 co-exposed to carbon nanopowder (CNPW) and BaP (Della Torre *et al.* 2017). In our study, only one
529 tissue (i.e. DG) has been analysed for BaP uptake making it difficult to a make a conclusion.

530 **Tracking MWCNTs in the mussel DG**

531 One of the most significant challenges when probing the uptake of nanoscale materials, including
532 carbon nanotubes, in marine biota is developing reliable and quantitative methods for their detection.
533 In this respect, CNTs represent a particular problem as their inherent structural polydispersity (i.e.
534 broad range of diameters and lengths) hinders conventional analytical approaches, such as
535 chromatographic separation. Moreover, methods based on elemental analysis and spectroscopic
536 techniques are generally not feasible because of the presence of organic matter. Spectrofluorometric
537 analysis is one approach that has been used successfully to quantify nanotubes in mouse cells and
538 rabbits (Cherukuri *et al.* 2004, 2006). However, as this technique is only applicable to semiconducting
539 SWCNTs. Insensitive to either individual metallic SWCNTs or bundles containing metallic SWCNTs, the
540 electronic properties and aggregation characteristics of nanotubes in environmental systems is often
541 unknown. This approach has therefore limited potential (O'Connell *et al.* 2002). Raman spectroscopy
542 was used to detect SWCNTs qualitatively in the aquatic organism *D. magna* (Roberts *et al.* 2007); yet,
543 this approach cannot provide quantitative results and is best suited for SWCNTs owing to the effects
544 of resonant signal enhancement. A method used recently to detect carbon nanotubes in biological
545 systems is tagging them with molecules that are either bonded to radioactive isotopes or are
546 themselves fluorescent (Kam *et al.* 2004, 2006, Singh *et al.* 2006). The use of such probes however
547 depends on the stability of its attachment to the nanotubes and, for radioactive labelling, attachment
548 of the isotope to the polymer. The addition of such bulky tags likely influences the physicochemical
549 properties of the nanotubes and thus their environmental behaviours.

550 The novel approach explored in our study was the utilisation of gold-labelled MWCNTs to improve the
551 traceability of nanotubes in biological samples. Indeed, ICP-MS results indicated the presence of gold
552 in mussel tissues, particularly in the digestive gland. Thus, bioaccumulation of MWCNTs in mussels at
553 the whole tissue level was confirmed, consistent with analogous previous studies using other aquatic
554 species (Templeton *et al.* 2006, Roberts *et al.* 2007, Smith *et al.* 2007, Ferguson *et al.* 2008, Petersen,
555 Akkanen, *et al.* 2009). In an attempt to probe the spatial location of labelled MWCNTs at the cellular
556 level, we analysed samples using electron microscopy. It is important to note that it has been shown
557 previously that incorrect sample preparation and subsequent image interpretation may lead to the

558 generation of false positives and inaccurate conclusions (Edgington *et al.* 2014). The most common
559 issue of this nature is that all high-contrast material presented in bright-field images of the sections
560 (where dark features correspond to structures comprising high atomic number elements) are assumed
561 to be from the specific artificial nanomaterial under examination. However, these may, in fact, be
562 related to unknown organic or inorganic matter or artefacts induced during the staining preparation
563 that is standard protocol for producing high quality transmission electron microscopy images. It is for
564 this reason that we elected to use gold-labelled nanotubes, in the absence of stains, in our studies.
565 This provided a uniquely diagnostic handle enabling us to correlate the presence of any foreign
566 materials with their exact elemental composition. Indeed, our combined electron microscopy and *in*
567 *situ* spectroscopy approach enabled us to show the presence of numerous metals in nanoparticle form
568 in both ESEM images of the whole tissues and STEM images of the digestive gland cross-sections from
569 control samples in the absence of labelled MWCNTs (Figures S5 and S7). Yet, despite an extensive
570 electron microscopy examination we were not able to visualise AuNP@MWCNTs in any of the samples
571 appraised (Figures S5 and S7). The absence of evidence from STEM/EDX analysis of the cross-section
572 is not unexpected given the large dimensions of the mussel (~5 mm²) relative to the size of the sections
573 (~180-200 nm in thickness). The fact that no evidence was observed in images of the whole tissue and
574 that gold is detected from bulk ICP-MS analysis means that MWCNTs must be located within the
575 internal structures of the DG. It suggests that the local probe nature of STEM confers a sampling issue,
576 though visualisation of their location at the cellular level remains elusive. These results emphasise the
577 challenge of direct imaging of nanostructures in biological samples and the importance of using a
578 range of different analytical techniques in order to obtain a good understanding of these complex
579 systems.

580 It should be noted that in our experiment the results were obtained at concentrations well above
581 environmentally realistic concentrations, especially for MWCNTs. As stated earlier, the predicted
582 environmental concentration for CNTs is at low ng/L. In a review, the assembled results from different
583 experiments indicate that carbon nanomaterials (CNMs) are not expected to be toxic to aquatic
584 organisms at environmentally relevant concentrations (Freixa *et al.* 2018). Toxic effects of CNMs to
585 aquatic organisms occur under high concentrations in short-term experiments (Jackson *et al.* 2013).
586 As stated in the review however (Freixa *et al.* 2018), in the near future numerous commercial products
587 are expected to include nanoparticles in their formulations (DeVolder *et al.* 2013), indicating that, the
588 concentration of CNMs in aquatic systems could increase to which organisms could be chronically
589 exposed. It should also be noted that the antagonistic response observed in the current study between
590 BaP and MWCNTs is based on a single concentration of the carbon nanotubes and as such represents
591 a general overview of potential toxicological behaviour. It is possible that this antagonistic interaction
592 could change when another concentration range is selected. Future studies must include more
593 realistic exposure scenarios to estimate accurately toxicity of nanomaterials.

594 **Conclusion**

595 Our findings highlight that impacts of the co-exposure of organic pollutants and CNTs on the
596 bioavailability and accumulation of the contaminants are mixed and species specific, indicating that in
597 the case of BaP the accumulation of this PAH is not facilitated by the presence of MWCNTs in *M.*
598 *galloprovincialis*. Environmentally realistic experiments are mandatory in order to identify and explain
599 the possible threat of ENMs to organisms. Many variables can modify the fate and consequently toxic
600 effects of ENPs and adsorbed pollutants. Fine characterisation of nanoparticles in (sea)water
601 (including characterisation of the adsorbed contaminants) and localization are the main challenge to

602 understand the toxic effect of this emerging contaminant in the environment. Overall, our study
603 demonstrate the challenges for hazard and risk assessments posed by ENMs and contribute to
604 improve our understanding of their potential interactive effects with other ubiquitous pollutants on
605 an ecologically an economically important marine organism.

606 **Acknowledgements**

607 We would like to thank Dr Alessandro La Torre (University of Nottingham) for technical support. The
608 views expressed in this article are those of the authors and not necessarily of the funding agencies
609 including the National Health Service, the National Institute for Health Research, the Department of
610 Health and Social Care or Public Health England.

611 **Disclosure statement**

612 The authors report no conflict of interest.

613 **Funding**

614 This study is mainly supported by Natural Environment Research Council (NERC), UK (Grant No.
615 NE/L006782/1; PI: ANJ). Additional Support from the Engineering and Physical Sciences Research
616 Council (EPSRC) [Grant No. EP/L022494/1] and the University of Nottingham is acknowledged. Work
617 at King's College London was further supported by the National Institute for Health Research Health
618 Protection Research Unit (NIHR HPRU) in Health Impact of Environmental Hazards at King's College
619 London in partnership with Public Health England (PHE) and Imperial College London.

620 **Word Count: 7918 (excluding references)**

621 **References**

- 622 Acevedo-Whitehouse, K., Cole, K.J., Phillips, D.H., Jepson, P.D., Deaville, R., and Arlt, V.M., 2018.
623 Hepatic DNA damage in harbour porpoises (*Phocoena phocoena*) stranded along the English
624 and Welsh coastlines. *Environmental and Molecular Mutagenesis*, 59 (7), 613–624.
- 625 Akcha, F., Burgeot, T., Venier, P., and Narbonne, J.F., 1999. Relationship between kinetics of
626 benzo[a]pyrene bioaccumulation and DNA binding in the mussel *Mytilus galloprovincialis*.
627 *Bulletin of Environmental Contamination and Toxicology*, 62 (4), 455–462.
- 628 Al-Subiaji, S.N., Arlt, V.M., Frickers, P.E., Readman, J.W., Stolpe, B., Lead, J.R., Moody, A.J., and Jha,
629 A.N., 2012. Merging nano-genotoxicology with eco-genotoxicology: An integrated approach to
630 determine interactive genotoxic and sub-lethal toxic effects of C 60 fullerenes and fluoranthene
631 in marine mussels, *Mytilus* sp. *Mutation Research - Genetic Toxicology and Environmental*

- 632 *Mutagenesis*, 745 (1–2), 92–103.
- 633 Anisimova, A.A., Chaika, V. V., Kuznetsov, V.L., and Golokhvast, K.S., 2015. Study of the influence of
634 multiwalled carbon nanotubes (12–14 nm) on the main target tissues of the bivalve *Modiolus*
635 *modiolus*. *Nanotechnologies in Russia*, 10 (3–4), 278–287.
- 636 Banni, M., Negri, A., Mignone, F., Boussetta, H., Viarengo, A., and Dondero, F., 2011. Gene
637 expression rhythms in the mussel *mytilus galloprovincialis* (Lam.) across an annual cycle. *PLoS*
638 *ONE*, 6 (5).
- 639 Banni, M., Sforzini, S., Arlt, V.M., Barranger, A., Dallas, L.J., Oliveri, C., Aminot, Y., Pacchioni, B.,
640 Millino, C., Lanfranchi, G., Readman, J.W., Moore, M.N., Viarengo, A., and Jha, A.N., 2017.
641 Assessing the impact of Benzo[a]pyrene on Marine Mussels: Application of a novel targeted
642 low density microarray complementing classical biomarker responses. *PLOS ONE*, 12 (6),
643 e0178460.
- 644 Barranger, A., Langan, L.M., Sharma, V., Rance, G.A., Aminot, Y., Weston, N.J., Akcha, F., Moore,
645 M.N., Arlt, V.M., Khlobystov, A.N., Readman, J.W., and Jha, A.N., 2019. Antagonistic
646 Interactions between Benzo[a]pyrene and Fullerene (C60) in Toxicological Response of Marine
647 Mussels. *Nanomaterials*, 9 (7), 987.
- 648 Baumard, P., Budzinski, H., and Garrigues, P., 1998. Environmental Chemistry POLYCYCLIC
649 AROMATIC HYDROCARBONS IN SEDIMENTS AND MUSSELS OF THE. *Environmental Toxicology*,
650 17 (5), 765–776.
- 651 Baumard, P., Budzinski, H., Garrigues, P., Dizer, H., and Hansen, P.D., 1999. Polycyclic aromatic
652 hydrocarbons in recent sediments and mussels (*Mytilus edulis*) from the Western Baltic Sea:
653 Occurrence, bioavailability and seasonal variations. *Marine Environmental Research*, 47 (1), 17–
654 47.
- 655 Beigbeder, A., Degee, P., Conlan, S.L., Mutton, R.J., Clare, A.S., Pettitt, M.E., Callow, M.E., Callow, J. a,
656 and Dubois, P., 2008. Preparation and characterisation of silicone-based coatings filled with
657 carbon nanotubes and natural sepiolite and their application as marine fouling-release
658 coatings. *Biofouling*, 24 (4), 291–302.
- 659 Bjorkland, R., Tobias, D.A., and Petersen, E.J., 2017. Increasing evidence indicates low

660 bioaccumulation of carbon nanotubes. *Environ. Sci.: Nano*, 4 (4), 747–766.

661 Bolognesi, C. and Fenech, M., 2012. Mussel micronucleus cytome assay. *Nature Protocols*, 7 (6),
662 1125–1137.

663 Brunk, U.T. and Terman, A., 2002. Lipofuscin: Mechanisms of age-related accumulation and
664 influence on cell function. *Free Radical Biology and Medicine*, 33 (5), 611–619.

665 Canesi, L., Ciacci, C., and Balbi, T., 2015. Interactive effects of nanoparticles with other contaminants
666 in aquatic organisms: Friend or foe? *Marine Environmental Research*, 111, 128–134.

667 Canesi, L., Ciacci, C., Vallotto, D., Gallo, G., Marcomini, A., and Pojana, G., 2010a. In vitro effects of
668 suspensions of selected nanoparticles (C60 fullerene, TiO₂, SiO₂) on *Mytilus* hemocytes.
669 *Aquatic Toxicology*, 96 (2), 151–158.

670 Canesi, L., Fabbri, R., Gallo, G., Vallotto, D., Marcomini, A., and Pojana, G., 2010b. Biomarkers in
671 *Mytilus galloprovincialis* exposed to suspensions of selected nanoparticles (Nano carbon black,
672 C60 fullerene, Nano-TiO₂, Nano-SiO₂). *Aquatic Toxicology*, 100 (2), 168–177.

673 Canesi, L., Frenzilli, G., Balbi, T., Bernardeschi, M., Ciacci, C., Corsolini, S., Della Torre, C., Fabbri, R.,
674 Faleri, C., Focardi, S., Guidi, P., Kočan, A., Marcomini, A., Mariottini, M., Nigro, M., Pozo-
675 Gallardo, K., Rocco, L., Scarcelli, V., Smerilli, A., and Corsi, I., 2014. Interactive effects of n-TiO₂
676 and 2,3,7,8-TCDD on the marine bivalve *Mytilus galloprovincialis*. *Aquatic Toxicology*, 153, 53–
677 65.

678 Canova, S., Degan, P., Peters, L., Livingstone, D., Voltan, R., and Venier, P., 1998. Tissue dose, DNA
679 adducts, oxidative DNA damage and CYP1A-immunopositive proteins in mussels exposed to
680 waterborne benzo[a]pyrene. *Mutation Research/Fundamental and Molecular Mechanisms of*
681 *Mutagenesis*, 399 (1), 17–30.

682 Cerrillo, C., Barandika, G., Igartua, A., Areitioaurtena, O., Marcaide, A., and Mendoza, G., 2015.
683 Ecotoxicity of multiwalled carbon nanotubes: Standardization of the dispersion methods and
684 concentration measurements. *Environmental Toxicology and Chemistry*, 34 (8), 1854–1862.

685 Cherukuri, P., Bachilo, S.M., Litovsky, S.H., and Weisman, R.B., 2004. Near-Infrared Fluorescence
686 Microscopy of Single-Walled Carbon Nanotubes in Phagocytic Cells. *Journal of the American*
687 *Chemical Society*, 126 (48), 15638–15639.

688 Cherukuri, P., Gannon, C.J., Leeuw, T.K., Schmidt, H.K., Smalley, R.E., Curley, S.A., and Weisman, R.B.,
689 2006. Mammalian pharmacokinetics of carbon nanotubes using intrinsic near-infrared
690 fluorescence. *Proceedings of the National Academy of Sciences*, 103 (50), 18882–18886.

691 Cho, K., Wang, X., Nie, S., Chen, Z., and Shin, D.M., 2008. Therapeutic nanoparticles for drug delivery
692 in cancer. *Clinical Cancer Research*, 14 (5), 1310–1316.

693 Conesa, A., Götz, S., García-Gómez, J.M., Terol, J., Talón, M., and Robles, M., 2005. Blast2GO: A
694 universal tool for annotation, visualization and analysis in functional genomics research.
695 *Bioinformatics*, 21 (18), 3674–3676.

696 D’Agata, A., Fasulo, S., Dallas, L.J., Fisher, A.S., Maisano, M., Readman, J.W., and Jha, A.N., 2014.
697 Enhanced toxicity of ‘bulk’ titanium dioxide compared to ‘fresh’ and ‘aged’ nano-TiO₂ in marine
698 mussels (*Mytilus galloprovincialis*). *Nanotoxicology*, 8 (5), 549–58.

699 Dallas, L.J., Bean, T.P., Turner, A., Lyons, B.P., and Jha, A.N., 2013. Oxidative DNA damage may not
700 mediate Ni-induced genotoxicity in marine mussels: assessment of genotoxic biomarkers and
701 transcriptional responses of key stress genes. *Mutation research*, 754 (1–2), 22–31.

702 David, R., Ebbels, T., and Gooderham, N., 2016. Synergistic and Antagonistic Mutation Responses of
703 Human MCL-5 Cells to Mixtures of Benzo[a]pyrene and 2-Amino-1-Methyl-6-
704 Phenylimidazo[4,5- b]pyridine: Dose-Related Variation in the Joint Effects of Common Dietary
705 Carcinogens. *Environmental Health Perspectives*, 124 (1), 88–96.

706 DellaTorre, C., Maggioni, D., Ghilardi, A., Parolini, M., Santo, N., Landi, C., Madaschi, L., Magni, S.,
707 Tasselli, S., Ascagni, M., Bini, L., La Porta, C., Del Giacco, L., and Binelli, A., 2018. The
708 interactions of fullerene C₆₀ and Benzo(A)pyrene influence their bioavailability and toxicity to
709 zebrafish embryos. *Environmental Pollution*, 241, 999–1008.

710 DellaTorre, C., Parolini, M., Del Giacco, L., Ghilardi, A., Ascagni, M., Santo, N., Maggioni, D., Magni, S.,
711 Madaschi, L., Prospero, L., La Porta, C., and Binelli, A., 2017. Adsorption of B(α)P on carbon
712 nanopowder affects accumulation and toxicity in zebrafish (*Danio rerio*) embryos.
713 *Environmental Science: Nano*, 4 (5).

714 DeMarchi, L., Neto, V., Pretti, C., Figueira, E., Chiellini, F., Soares, A.M.V.M., and Freitas, R., 2017a.
715 Physiological and biochemical responses of two keystone polychaete species: *Diopatra*

716 neapolitana and Hediste diversicolor to Multi-walled carbon nanotubes. *Environmental*
717 *Research*, 154 (December 2016), 126–138.

718 DeMarchi, L., Neto, V., Pretti, C., Figueira, E., Chiellini, F., Soares, A.M.V.M., and Freitas, R., 2017b.
719 The impacts of emergent pollutants on Ruditapes philippinarum: biochemical responses to
720 carbon nanoparticles exposure. *Aquatic Toxicology*, 187, 38–47.

721 DeVolder, M.F.L., Tawfick, S.H., Baughman, R.H., and Hart, J.A., 2013. Carbon nanotubes: present
722 and future commercial applications. *Science.*, 339 (February), 535–539.

723 Di, Y., Aminot, Y., Schroeder, D.C., Readman, J.W., and Jha, A.N., 2016. Integrated biological
724 responses and tissue-specific expression of p53 and ras genes in marine mussels following
725 exposure to benzo(α)pyrene and C60 fullerenes, either alone or in combination. *Mutagenesis*,
726 00, 1–14.

727 Di, Y., Schroeder, D.C., Highfield, A., Readman, J.W., and Jha, A.N., 2011. Tissue-specific expression of
728 p53 and ras genes in response to the environmental genotoxicant benzo(a)pyrene in marine
729 mussels. *Environmental Science and Technology*, 45 (20), 8974–8981.

730 Edgington, A.J., Petersen, E.J., Herzing, A.A., Podila, R., Rao, A., and Klaine, S.J., 2014. Microscopic
731 investigation of single-wall carbon nanotube uptake by *Daphnia magna*. *Nanotoxicology*, 8
732 (sup1), 2–10.

733 Ferguson, P.L., Chandler, G.T., Templeton, R.C., Demarco, A., Scrivens, W.A., and Englehart, B.A.,
734 2008. Influence of sediment - Amendment with single-walled carbon nanotubes and diesel soot
735 on bioaccumulation of hydrophobic organic contaminants by benthic invertebrates.
736 *Environmental Science and Technology*, 42 (10), 3879–3885.

737 Foss Hansen, S., Heggelund, L.R., Revilla Besora, P., Mackevica, A., Boldrin, A., and Baun, A., 2016.
738 Nanoproducts - What is actually available to European consumers? *Environmental Science:*
739 *Nano*, 3 (1), 169–180.

740 Freixa, A., Acuña, V., Sanchís, J., Farré, M., Barceló, D., and Sabater, S., 2018. Ecotoxicological effects
741 of carbon based nanomaterials in aquatic organisms. *Science of The Total Environment*, 619–
742 620, 328–337.

743 Galloway, T., Lewis, C., Dolciotti, I., Johnston, B.D., Moger, J., and Regoli, F., 2010. Sublethal toxicity

744 of nano-titanium dioxide and carbon nanotubes in a sediment dwelling marine polychaete.
745 *Environmental Pollution*, 158 (5), 1748–1755.

746 Giese, B., Klaessig, F., Park, B., Kaegi, R., Steinfeldt, M., Wigger, H., Von Gleich, A., Gottschalk, F.,
747 2018. Risks, release and concentrations of engineered nanomaterials in the environment.
748 *Scientific Reports* 8: 1565.

749 Goldberg, E.D., 1987. Heavy metal analyses in the marine environment - approaches to quality
750 control. *Marine Chemistry*, 22 (2–4), 117–124.

751 Gomes, T., Araújo, O., Pereira, R., Almeida, A.C., Cravo, A., and Bebianno, M.J., 2013. Genotoxicity of
752 copper oxide and silver nanoparticles in the mussel *Mytilus galloprovincialis*. *Marine*
753 *Environmental Research*, 84, 51–59.

754 Gottschalk, F., Sun, T., and Nowack, B., 2013. Environmental concentrations of engineered
755 nanomaterials: Review of modeling and analytical studies. *Environmental Pollution*, 181, 287–
756 300.

757 Halldórsson, H.P., De Pirro, M., Romano, C., Svavarsson, J., and Sarà, G., 2008. Immediate biomarker
758 responses to benzo[a]pyrene in polluted and unpolluted populations of the blue mussel
759 (*Mytilus edulis* L.) at high-latitudes. *Environment International*, 34 (4), 483–489.

760 Hu, X., Li, J., Chen, Q., Lin, Z., and Yin, D., 2014. Combined effects of aqueous suspensions of
761 fullerene and humic acid on the availability of polycyclic aromatic hydrocarbons: Evaluated
762 with negligible depletion solid-phase microextraction. *Science of The Total Environment*, 493,
763 12–21.

764 Hu, X., Liu, J., Mayer, P., and Jiang, G., 2008. Impacts of some environmentally relevant parameters
765 on the sorption of polycyclic aromatic hydrocarbons to aqueous suspensions of fullerene.
766 *Environmental Toxicology and Chemistry*, 27 (9), 1868.

767 Hutchison, G.R., Christensen, F.M., Aschberger, K., Johnston, H.J., Hankin, S., Stone, V., and Peters,
768 S., 2010. A critical review of the biological mechanisms underlying the in vivo and in vitro
769 toxicity of carbon nanotubes: The contribution of physico-chemical characteristics .
770 *Nanotoxicology*, 4 (2), 207–246.

771 Jackson, P., Jacobsen, N.R., Baun, A., Birkedal, R., Kühnel, D., Jensen, K.A., Vogel, U., and Wallin, H.,

772 2013. Bioaccumulation and ecotoxicity of carbon nanotubes. *Chemistry Central Journal*, 7 (1),
773 154.

774 Kam, N.W.S., Jessop, T.C., Wender, P.A., and Dai, H., 2004. Nanotube molecular transporters:
775 Internalization of carbon nanotube-protein conjugates into mammalian cells. *Journal of the*
776 *American Chemical Society*, 126 (22), 6850–6851.

777 Kam, N.W.S., Liu, Z., and Dai, H., 2006. Carbon nanotubes as intracellular transporters for proteins
778 and DNA: An investigation of the uptake mechanism and pathway. *Angewandte Chemie -*
779 *International Edition*, 45 (4), 577–581.

780 Katsifis, S.P., Kinney, P.L., Hosselet, S., Burns, F.J., and Christie, N.T., 1996. Interaction of nickel with
781 mutagens in the induction of sister chromatid exchanges in human lymphocytes. *Mutation*
782 *Research/Environmental Mutagenesis and Related Subjects*, 359 (1), 7–15.

783 LaTorre, A., Rance, G. a., El Harfi, J., Li, J., Irvine, D.J., Brown, P.D., and Khlobystov, A.N., 2010.
784 Transport and encapsulation of gold nanoparticles in carbon nanotubes. *Nanoscale*, 2, 1006–
785 1010.

786 Linard, E.N., Apul, O.G., Karanfil, T., Van Den Hurk, P., and Klaine, S.J., 2017. Bioavailability of Carbon
787 Nanomaterial-Adsorbed Polycyclic Aromatic Hydrocarbons to *Pimphales promelas*: Influence of
788 Adsorbate Molecular Size and Configuration. *Environmental Science and Technology*, 51 (16),
789 9288–9296.

790 Livingstone, D.R. and Pipe, R.K., 1992. Mussels and environmental contaminants: molecular and
791 cellular aspects. *Dev. Aquac. Fish. Sci*, 25, 424–464.

792 Maruyama, K., Haniu, H., Saito, N., Matsuda, Y., Tsukahara, T., Kobayashi, S., Tanaka, M., Aoki, K.,
793 Takanashi, S., Okamoto, M., and Kato, H., 2015. Endocytosis of multiwalled carbon nanotubes
794 in bronchial epithelial and mesothelial cells. *BioMed Research International*, 2015.

795 Maurer-Jones, M.A., Gunsolus, I.L., Murphy, C.J., and Haynes, C.L., 2013. Toxicity of engineered
796 nanoparticles in the environment. *Analytical Chemistry*, 85 (6), 3036–3049.

797 Miners, S.A., Rance, G.A., and Khlobystov, A.N., 2016. Chemical reactions confined within carbon
798 nanotubes. *Chemical Society Reviews*, 45 (17), 4727–4746.

- 799 Miners, S.A., Rance, G.A., La Torre, A., Kenny, S.M., and Khlobystov, A.N., 2014. Controlled oxidative
800 cutting of carbon nanotubes catalysed by silver nanoparticles. *Journal of Materials Chemistry C*,
801 2 (39), 8357–8363.
- 802 Moore, M.N., Depledge, M.H., Readman, J.W., and Paul Leonard, D.R., 2004. An integrated
803 biomarker-based strategy for ecotoxicological evaluation of risk in environmental
804 management. *Mutation Research - Fundamental and Molecular Mechanisms of Mutagenesis*,
805 552 (1–2), 247–268.
- 806 Moore, M.N., Viarengo, A., Donkin, P., and Hawkins, A.J.S., 2007. Autophagic and lysosomal
807 reactions to stress in the hepatopancreas of blue mussels. *Aquatic Toxicology*, 84 (1), 80–91.
- 808 Moore, M.N., Wedderburn, J., Clarke, K.R., McFadzen, I., Lowe, D.M., Readman, J.W. 2018. Emergent
809 synergistic lysosomal toxicity of chemical mixtures in molluscan blood cells (hemocytes).
810 *Environmental Pollution*, 235, 1006-1014.
- 811 Negri, A., Oliveri, C., Sforzini, S., Mignione, F., Viarengo, A., and Banni, M., 2013. Transcriptional
812 Response of the Mussel *Mytilus galloprovincialis* (Lam.) following Exposure to Heat Stress and
813 Copper. *PLoS ONE*, 8 (6).
- 814 Nel, A., Xia, T., Mädler, L., and Li, N., 2006. Toxic potential of materials at the nanolevel. *Science*.
- 815 Nikolaou, A., Kostopoulou, M., Petsas, A., Vagi, M., Lofrano, G., and Meric, S., 2009. Levels and
816 toxicity of polycyclic aromatic hydrocarbons in marine sediments. *TrAC - Trends in Analytical*
817 *Chemistry*, 28 (6), 653–664.
- 818 O’Connell, M.J., Bachilo, S.M., Huffman, C.B., Moore, V.C., Strano, M.S., Haroz, E.H., Rialon, K.L.,
819 Boul, P.J., Noon, W.H., Kittrell, C., Ma, J., Hauge, R.H., Weisman, R.B., and Smalley, R.E., 2002.
820 Band Gap Fluorescence from Individual Single-Walled Carbon Nanotubes. *Science*, 297 (5581),
821 593 LP – 596.
- 822 Park, J.-W., Henry, T.B., Ard, S., Menn, F.-M., Compton, R.N., and Sayler, G.S., 2011. The association
823 between nC(60) and 17 α -ethinylestradiol (EE2) decreases EE2 bioavailability in zebrafish and
824 alters nanoaggregate characteristics. *Nanotoxicology*, 5 (September), 406–416.
- 825 Petersen, E.J., Akkanen, J., Kukkonen, J.V.K., and Weber, W.J., 2009a. Biological uptake and
826 depuration of carbon nanotubes by *daphnia magna*. *Environmental Science and Technology*, 43

827 (8), 2969–2975.

828 Petersen, E.J., Pinto, R.A., Landrum, P.F., and Weber, W.J., 2009b. Influence of Carbon Nanotubes on
829 Pyrene Bioaccumulation from Contaminated Soils by Earthworms. *Environmental Science &*
830 *Technology*, 43 (11), 4181–4187.

831 Phillips, D.H. and Arlt, V.M., 2014. 32P-Postlabeling Analysis of DNA Adducts. *In*: P. Keohavong and
832 S.G. Grant, eds. *Molecular Toxicology Protocols*. Totowa, NJ: Humana Press, 127–138.

833 Plant, A.L., Benson, D.M., and Smith, L.C., 1985. Cellular uptake and intracellular localization of
834 benzo(a)pyrene by digital fluorescence imaging microscopy. *Journal of Cell Biology*, 100 (4),
835 1295–1308.

836 Rance, G.A., Marsh, D.H., and Khlobystov, A.N., 2008. Extinction coefficient analysis of small
837 alkanethiolate-stabilised gold nanoparticles. *Chemical Physics Letters*, 460 (1–3), 230–236.

838 Rashid, F., Horobin, R.W., and Williams, M.A., 1991. Predicting the behaviour and selectivity of
839 fluorescent probes for lysosomes and related structures by means of structure-activity models.
840 *The Histochemical Journal*, 23 (10), 450–459.

841 Roberts, A.P., Mount, A.S., Seda, B., Souther, J., Qiao, R., Lin, S., Pu, C.K., Rao, A.M., and Klaine, S.J.,
842 2007. In vivo biomodification of lipid-coated carbon nanotubes by *Daphnia magna*.
843 *Environmental Science and Technology*, 41 (8), 3028–3029.

844 Rocha, T.L., Gomes, T., Sousa, V.S., Mestre, N.C., and Bebianno, M.J., 2015. Ecotoxicological impact
845 of engineered nanomaterials in bivalve molluscs: An overview. *Marine Environmental Research*,
846 111, 74–88.

847 Sayes, C.M., Fortner, J.D., Guo, W., Lyon, D., Boyd, A.M., Ausman, K.D., Tao, Y.J., Sitharaman, B.,
848 Wilson, L.J., Hughes, J.B., West, J.L., and Colvin, V.L., 2004. The Differential Cytotoxicity of
849 Water-Soluble Fullerenes. *Nano Letters*, 4 (10), 1881–1887.

850 Schlesinger, R.B., Zelikoff, J.T., Chen, L.C., and Kinney, P.L., 1992. Assessment of toxicologic
851 interactions resulting from acute inhalation exposure to sulfuric acid and ozone mixtures.
852 *Toxicology and Applied Pharmacology*, 115 (2), 183–190.

853 Schwartz, D. and Rotter, V., 1998. P53-Dependent Cell Cycle Control: Response To Genotoxic Stress.

- 854 *Seminars in cancer biology*, 8 (5), 325–336.
- 855 Sforzini, S., Moore, M.N., Oliveri, C., Volta, A., Jha, A., Banni, M., and Viarengo, A., 2018a. Role of
856 mTOR in autophagic and lysosomal reactions to environmental stressors in molluscs. *Aquatic*
857 *Toxicology*, 195 (December 2017), 114–128.
- 858 Sforzini, S., Oliveri, C., Orrù, A., Chessa, G., Pacchioni, B., Millino, C., Jha, A.N., Viarengo, A., and
859 Banni, M., 2018b. Application of a new targeted low density microarray and conventional
860 biomarkers to evaluate the health status of marine mussels: A field study in Sardinian coast,
861 Italy. *Science of The Total Environment*, 628–629, 319–328.
- 862 Shaw, J.P., Large, A.T., Donkin, P., Evans, S. V, Staff, F.J., Livingstone, D.R., Chipman, J.K., and Peters,
863 L.D., 2004. Seasonal variation in cytochrome P450 immunopositive protein levels, lipid
864 peroxidation and genetic toxicity in digestive gland of the mussel *Mytilus edulis*. *Aquatic*
865 *Toxicology*, 67 (4), 325–336.
- 866 Singh, R., Pantarotto, D., Lacerda, L., Pastorin, G., Klumpp, C., Prato, M., Bianco, A., and Kostarelos,
867 K., 2006. Tissue biodistribution and blood clearance rates of intravenously administered carbon
868 nanotube radiotracers. *Proceedings of the National Academy of Sciences*, 103 (9), 3357–3362.
- 869 Smith, C.J., Shaw, B.J., and Handy, R.D., 2007. Toxicity of single walled carbon nanotubes to rainbow
870 trout, (*Oncorhynchus mykiss*): Respiratory toxicity, organ pathologies, and other physiological
871 effects. *Aquatic Toxicology*, 82 (2), 94–109.
- 872 Sogbanmu, T.O., Nagy, E., Phillips, D.H., Arlt, V.M., Otitolaju, A.A., and Bury, N.R., 2016. Lagos lagoon
873 sediment organic extracts and polycyclic aromatic hydrocarbons induce embryotoxic,
874 teratogenic and genotoxic effects in *Danio rerio* (zebrafish) embryos. *Environ Sci Pollut Res Int.*
- 875 Solé, M., Porte, C., and Albaigés, J., 1995. Seasonal variation in the mixed-function oxygenase system
876 and antioxidant enzymes of the mussel *Mytilus galloprovincialis*. *Environmental Toxicology and*
877 *Chemistry*, 14 (1), 157–164.
- 878 Su, Y., Yan, X., Pu, Y., Xiao, F., Wang, D., and Yang, M., 2013. Risks of single-walled carbon nanotubes
879 acting as contaminants-carriers: Potential release of phenanthrene in Japanese medaka
880 (*Oryzias latipes*). *Environmental Science and Technology*, 47 (9), 4704–4710.
- 881 Sun, H., Ruan, Y., Zhu, H., Zhang, Z., Zhang, Y., and Yu, L., 2014. Enhanced bioaccumulation of

882 pentachlorophenol in carp in the presence of multi-walled carbon nanotubes. *Environmental*
883 *Science and Pollution Research*, 21 (4), 2865–2875.

884 Sun, T.Y., Bornhöft, N.A., Hungerbühler, K., and Nowack, B., 2016. Dynamic Probabilistic Modeling of
885 Environmental Emissions of Engineered Nanomaterials. *Environmental Science and Technology*,
886 50 (9), 4701–4711.

887 Templeton, R.C., Ferguson, P.L., Washburn, K.M., Scrivens, W.A., and Chandler, G.T., 2006. Life-cycle
888 effects of single-walled carbon nanotubes (SWNTs) on an estuarine meiobenthic copepod.
889 *Environmental Science and Technology*, 40 (23), 7387–7393.

890 VanBerlo, D., Clift, M., Albrecht, C., and Schins, R., 2012. Carbon nanotubes: An insight into the
891 mechanisms of their potential genotoxicity. *Swiss Medical Weekly*, 142 (November), 1–16.

892 Vernon, E.L. and Jha, A.N., 2019. Assessing relative sensitivity of marine and freshwater bivalves
893 following exposure to copper: Application of classical and novel genotoxicological biomarkers.
894 *Mutation Research - Genetic Toxicology and Environmental Mutagenesis*, 842 (January), 60–71.

895 Xia, X., Chen, X., Zhao, X., Chen, H., and Shen, M., 2012. Effects of carbon nanotubes, chars, and ash
896 on bioaccumulation of perfluorochemicals by chironomus plumosus larvae in sediment.
897 *Environmental Science and Technology*, 46 (22), 12467–12475.

898 Xu, H., Cheng, X., Zhong, J., Meng, J., Yang, M., Jia, F., Xu, Z., and Kong, H., 2011. Characterization of
899 multiwalled carbon nanotubes dispersing in water and association with biological effects.
900 *Journal of Nanomaterials*, 2011.

901 Yang, K., Wang, X., Zhu, L., and Xing, B., 2006. Competitive Sorption of Pyrene, Phenanthrene, and
902 Naphthalene on Multiwalled Carbon Nanotubes. *Environmental Science & Technology*, 40 (18),
903 5804–5810.

904 Zangar, R.C., Davydov, D.R., and Verma, S., 2004. Mechanisms that regulate production of reactive
905 oxygen species by cytochrome P450. *Toxicology and Applied Pharmacology*, 199 (3), 316–331.

906 Zhang, S., Zhang, J., Chen, H., Wang, A., Liu, Y., Hou, H. & Hu, Q. (2019). Combined cytotoxicity of co-
907 exposure to aldehyde mixtures on human bronchial epithelial BEAS-2B cells. *Environmental*
908 *Pollution*, 250, 250-261.

909

910

911 **Table 1.** Chemical analyses of the mussel digestive gland after the 3-day exposure to BaP and
 912 MWCNTs.

Treatments	Water content (% wet weight)	BaP concentration ($\mu\text{g g}^{-1}$ dry weight)
Solvent control	77.1 \pm 2.2	< 0.5
Solvent control + MWCNT 1mg L⁻¹	78.8 \pm 2.1	< 0.5
BaP 5 $\mu\text{g L}^{-1}$	78.7 \pm 2.6	6.9 \pm 2.1
BaP 50 $\mu\text{g L}^{-1}$	76.1 \pm 1.8	163.2 \pm 68.4
BaP 100 $\mu\text{g L}^{-1}$	75.7 \pm 3.8	475.0 \pm 45.7
MWCNT + BaP 5 $\mu\text{g L}^{-1}$	78.0 \pm 3.5	6.0 \pm 2.6
MWCNT + BaP 50 $\mu\text{g L}^{-1}$	77.6 \pm 3.2	36.1 \pm 23.1*
MWCNT + BaP 100 $\mu\text{g L}^{-1}$	77.9 \pm 3.2	267.9 \pm 6.4*

913

914 Asterisks indicate the statistical differences observed between treatments exposed to BaP only and
 915 treatments exposed to BaP + MWCNTs. (*) $p < 0.05$.

916

917 **Table 2.** Number of DEGs depicted in mussels exposed to BaP alone and with MWCNTs against control (DMSO). Shown are numbers of up- and down-
918 regulated DEGs.

		BaP 5 $\mu\text{g L}^{-1}$	BaP 50 $\mu\text{g L}^{-1}$	BaP 100 $\mu\text{g L}^{-1}$	MWCNT	MWCNT + BaP 5 $\mu\text{g L}^{-1}$	MWCNT + BaP 50 $\mu\text{g L}^{-1}$	MWCNT + BaP 100 $\mu\text{g L}^{-1}$
Gills	Up	2	8	6	1	8	6	9
	Down	1	3	3	3	6	4	5
DG	Up	7	4	5	3	3	8	4
	Down	7	1	7	1	2	3	1

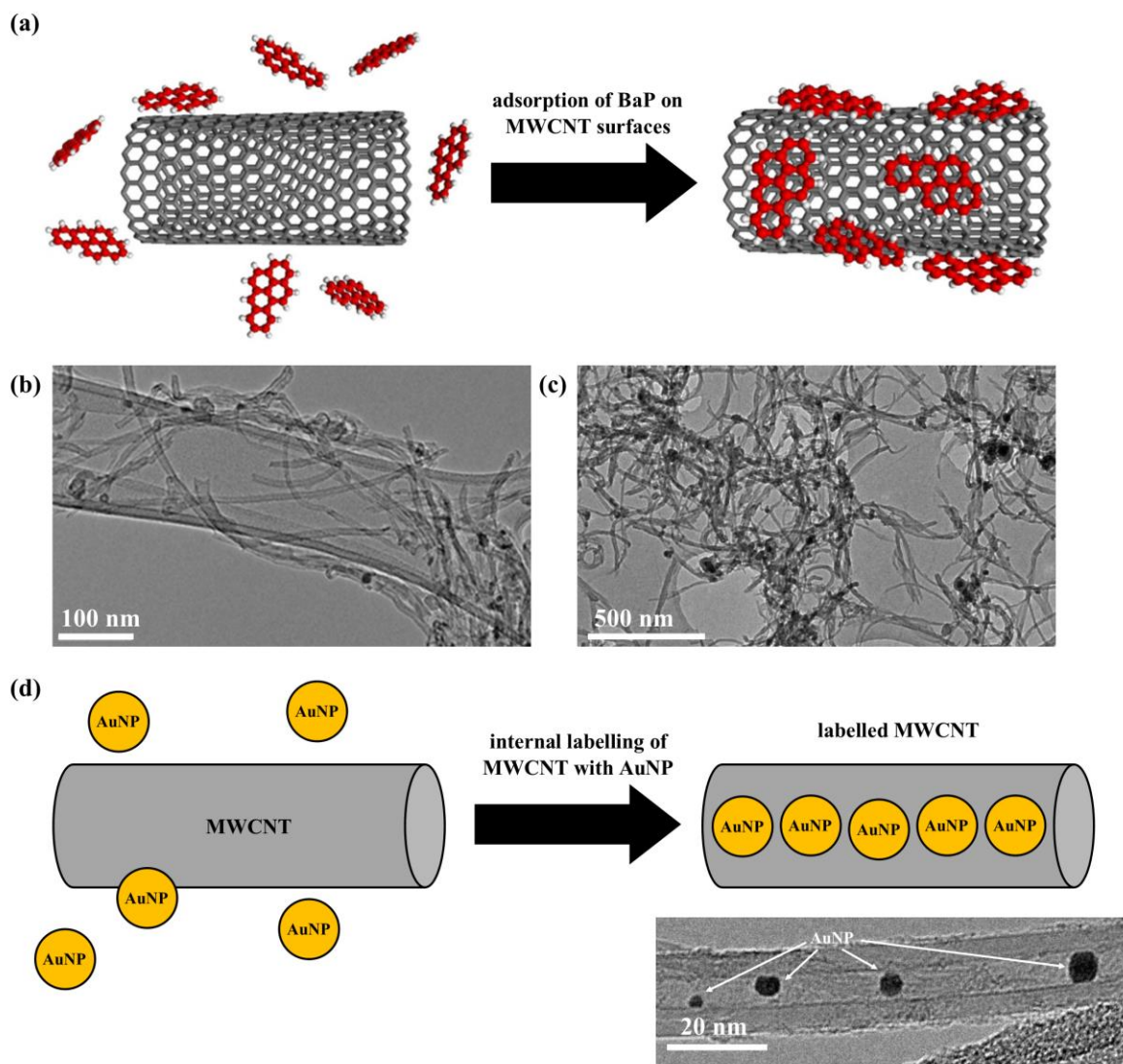
919 **Table 3.** Analysis of combined effects of MWCNT and BaP on DNA Damage (Comet assay) based on
920 Interaction Factors (IF).

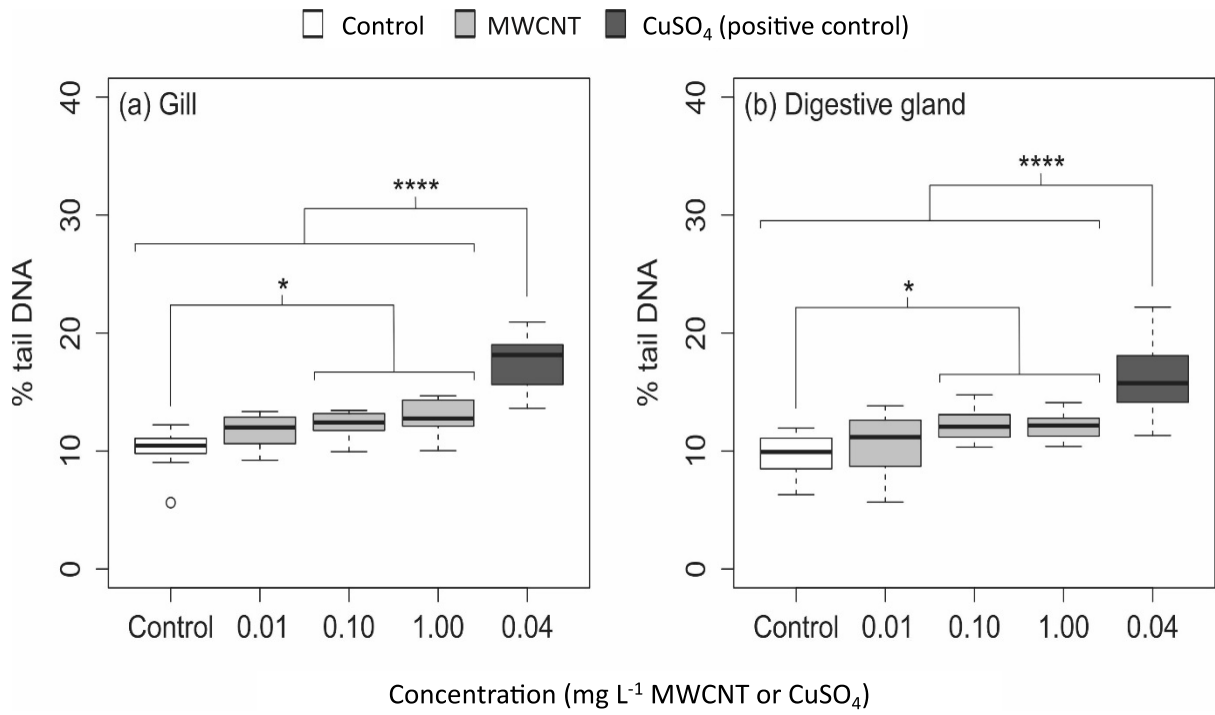
Treatments	Interaction Factors for DNA Damage (Comet Assay)
MWCNT 1 mg L ⁻¹ + BaP 5µg L ⁻¹	-396.42 ± 174.57
MWCNT 1 mg L ⁻¹ + BaP 50 µg L ⁻¹	-438.38* ± 297.56
MWCNT 1 mg L ⁻¹ + BaP 100 µg L ⁻¹	-505.92* ± 166.69

921

922 Interaction Factor ± 95% Confidence Limit / $\sqrt{2}$ (Moore et al., 2018). * indicates significance at the 5%
923 level. A negative **IF** indicates antagonism; an **IF** of 0 indicates additivity; and a positive **IF** indicates
924 synergism.

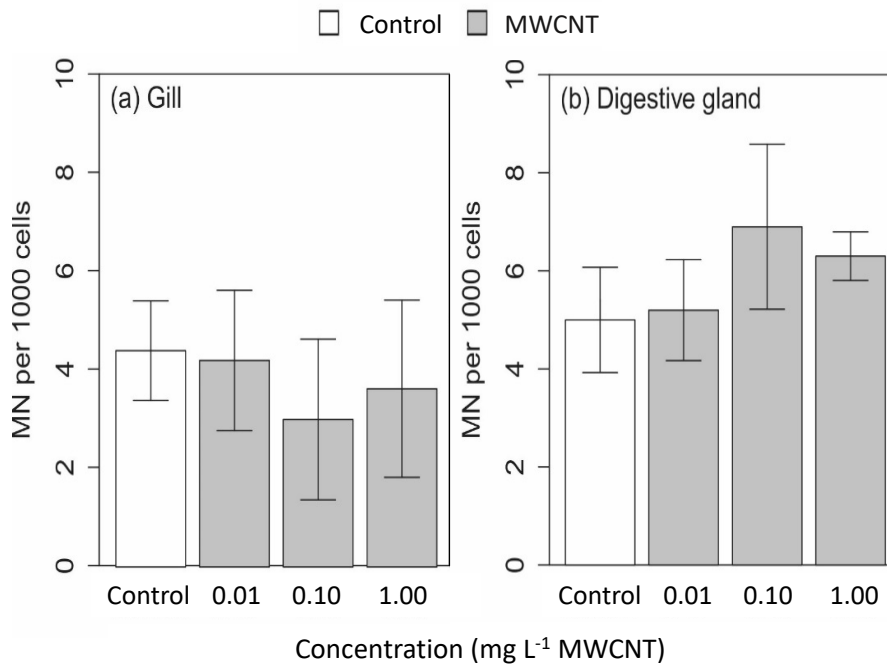
925





929

930 Figure 2



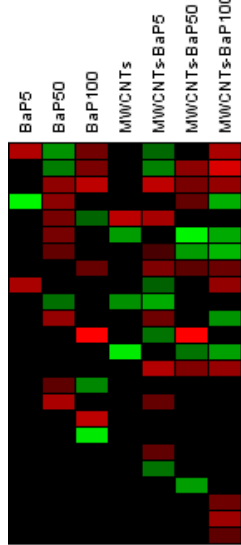
931

932

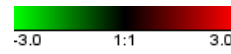
933 **Figure 3**



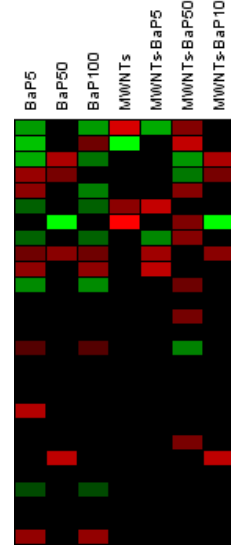
(a) Gill



p63/p73-like protein
 member ras oncogene family
 caspase 3/7-4 mRNA
 guanine nucleotide binding2
 p53 tumor suppressor-like protein (p53)
 t-cell lymphoma invasion and metastasis 1
 Mytilus edulis RAS
 putative caspase 3 mRNA
 death-associated protein kinase 1
 member ras oncogene family
 dna ligase i
 alkaline phosphatase
 delta-n p63 p73-like protein
 defender against cell death 1
 h2a histonemember z
 caspase 8 mRNA
 caspase 3/7-3 mRNA
 h3family 3b
 adp-ribosylation factor 1
 caspase 2 mRNA
 Mytilus edulis topoisomerase II
 Bcl-2-associated X
 TNF receptor-associated
 Bax inhibitor-1 protein (BI1)



(b) Digestive gland

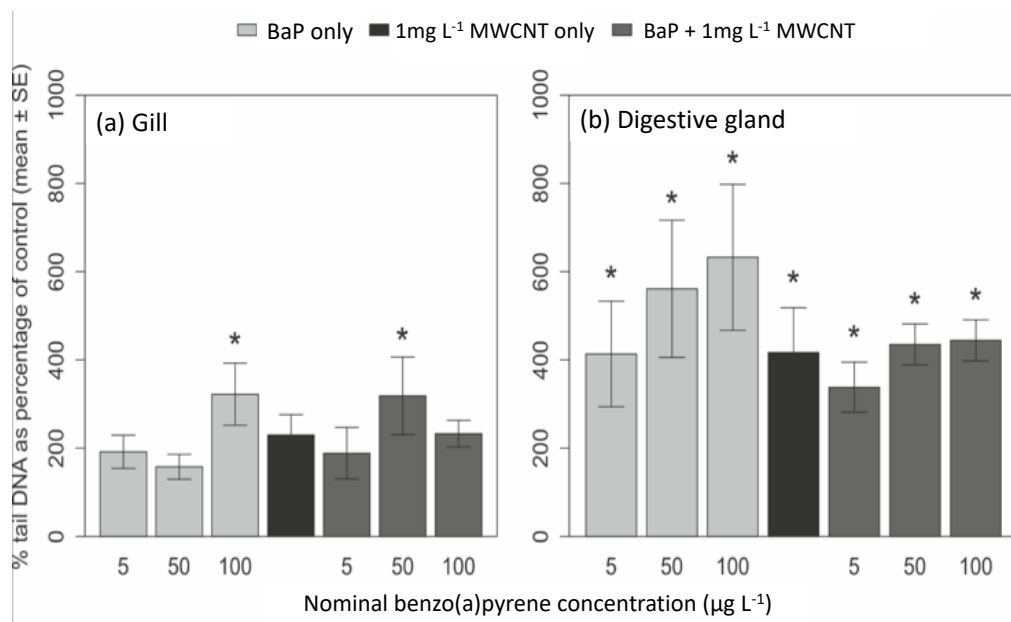


p63/p73-like protein
 caspase 3/7-4 mRNA
 h2a histonemember z
 p53 tumor suppressor-like protein (p53)
 defender against cell death 1
 dna ligase i
 alkaline phosphatase
 TNF receptor-associated
 Mytilus edulis RAS mRNA,
 guanine nucleotide binding2
 delta-N p63/p73-like protein
 Mytilus trossulus MDM-like
 p63/p73-like protein
 member ras oncogene family
 t-cell lymphoma invasion and metastasis 1
 member ras oncogene family
 death-associated protein kinase 1
 adp-ribosylation factor 1
 Bax inhibitor-1 protein (BI1)
 caspase 3/7-3 mRNA
 caspase 2 mRNA
 h3family 3b
 Mytilus edulis p53 tumor suppressor-like protein
 Mytilus galloprovincialis gadd45a
 histone aminotransferase 1
 putative caspase 3 mRNA
 Mytilus edulis topoisomerase II mRNA,

934

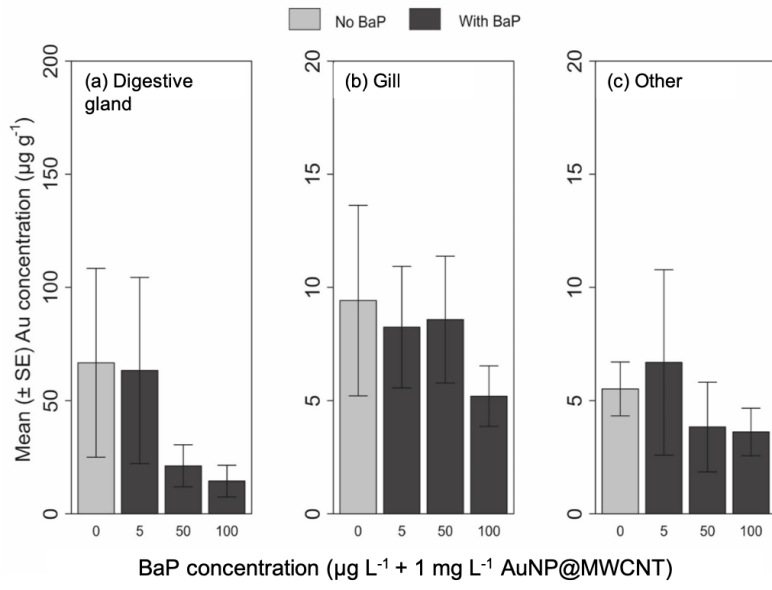
935 **Figure 4**

936



937

938 **Figure 5**



939

940 **Figure 6**

941 **Figure legends and Table captions**

942 **Figure 1.** (a) Schematic diagram illustrating the adsorption of BaP onto the exterior surfaces of
943 MWCNTs due to strong and specific van der Waals interactions. (b) TEM image of MWCNTs used in
944 the experiments with BaP. (c) TEM image of MWCNT aggregates in seawater. In both (b) and (c),
945 aggregated MWCNTs are observed as a consequence of the drying procedure employed during TEM
946 sample preparation; however, MWCNTs appear more aggregated in the presence of seawater, as
947 confirmed by light scattering analysis of the suspension of MWCNTs in seawater (Figure S1). (d)
948 Schematic diagram illustrating the labelling of MWCNTs by insertion of AuNPs into the nanotube
949 cavity that have been employed as diagnostic markers for the presence of MWCNTs in the
950 experiments with BaP. A corresponding TEM image of AuNP@MWCNT with arrows denoting the
951 positions of the confined AuNPs.

952 **Figure 2.** Levels of DNA damage as measured by the Comet assay in the mussel tissues after the 7-
953 day exposure to MWCNTs. Asterisks indicate the statistical differences observed between control
954 and exposed groups. (*) $p < 0.05$, (**) $p < 0.01$, (***) $p < 0.001$.

955 **Figure 3.** Levels of micronuclei in the mussel tissues after the 7-day exposure to MWCNTs.

956 **Figure 4.** Gene expression profile of gill (a) and DG (b) tissues in animals exposed to increasing BaP
957 concentrations (5, 50 and $100 \mu\text{g L}^{-1}$) and their combination with MWCNTs (1 mg L^{-1}). The heat map
958 reports log₂ relative expression level with respect to the reference condition. 24 and 27 DEGs were
959 generated in at least one condition for gill and DG respectively. Microarray data was analysed using
960 the Linear Mode for Microarray Analysis (LIMMA) software as described in Banni et al, (2011). B
961 statistics with adjusted p-value, 0.05 and B.0 were used as a threshold for rejection of the null
962 hypothesis (no variation).

963 **Figure 5.** Levels of DNA damage as measured by the Comet assay in mussel tissues after 3-day
964 exposure to BaP with and without co-exposure to 1 mg L^{-1} MWCNT. Data are expressed as % control
965 values (not shown) in order to standardise across two different sampling days. Asterisks indicate
966 significant differences from the same tissues in control mussels.

967 **Figure 6.** Gold concentration in mussel (a) gill, (b) DG and (c) other tissues (mean \pm SE) after the 3-
968 day exposure to 1 mg L^{-1} gold-labelled MWCNT (AuNP@MWCNT), with and without co-exposure to
969 BaP. Regarding DG, the highest Au level in the absence and presence of BaP at a concentration of 5

970 $\mu\text{g L}^{-1}$ are due to single outliers. Non-parametric statistical test (Kruskal-Wallis) indicated no
971 significant differences (p-value= 0.3256).

972 **Table 2.** Chemical analyses of the mussel digestive gland after the 3-day exposure to BaP and
973 MWCNTs.

974 **Table 2.** Number of DEGs depicted in mussels exposed to BaP alone and with MWCNTs against
975 control (DMSO). Shown are numbers of up- and down-regulated DEGs.

976 **Table 3.** Analysis of combined effects of MWCNT and BaP on DNA Damage (Comet assay) based on
977 Interaction Factors (IF).

978 **Figure S1.** The hydrodynamic diameter (d_H) of (a) MWCNT in mussel-exposed seawater (1541 ± 193
979 nm), MWCNT in seawater (1666 ± 198 nm) and (c) MWCNT + BaP (1642 ± 431 nm) in mussel-exposed
980 seawater, as determined by DLS. Whilst the maximum possible concentration of MWCNTs in
981 seawater in all experiments is 0.1 mg mL^{-1} , concentrations of the stable suspensions within the range
982 $\sim 0.01\text{-}0.02 \text{ mg mL}^{-1}$ ($\sim 10\text{-}20 \text{ mg L}^{-1}$) were determined using a spectrophotometric approach
983 developed within our group previously (Marsh *et al.* 2007), which is an order of magnitude higher
984 than the concentration utilised in the highest exposure experiment, but at the lower limit of the
985 concentration range detectable using the particle sizing instrumentation. The concentration of BaP
986 in seawater in the latter experiment is 0.001 mg mL^{-1} . Control measurements of seawater in the
987 absence of MWCNTs yielded no measurable scatterers.

988 **Figure S2.** (a) TEM and (b) EDX spectroscopy analysis of MWCNTs in seawater. TEM indicates the
989 likelihood of micron-sized MWCNT aggregates in suspension which afford extended web-like
990 ensembles as they deposit onto the carbon films during TEM sample preparation. The EDX spectrum
991 is dominated by C (MWCNT and the grid support film), with smaller signals from Si and O (from silica,
992 a likely contaminant found in seawater). The presence of Cu is associated with the TEM grid and
993 column assembly.

994 **Scheme S1.** Schematic representation of the preparation of AuNP@MWCNT.

995 **Figure S3.** Electron microscopy and *in situ* spectroscopy analysis of AuNP@MWCNT. (a) Bright field
996 TEM image (top) and corresponding STEM/EDX map confirming the presence of Au (bottom). (b) EDX
997 spectra captured from the area shown in (a) indicating the composition of the dark features in the
998 bright field image correspond to AuNPs.

999 **Table S1.** The concentration of BaP in seawater at day 1 (1 h after dosing) and day 3 (at the end of
1000 the exposure). Data are means \pm SE (n = 3) for the BaP 50 treatment.

1001 **Table S2:** Q-PCR primers and Taqman probes

1002 **Table S3:** M-Values of DEGs in gills of mussels exposed to increasing BaP concentrations ($5 \mu\text{g L}^{-1}$, 50
1003 $\mu\text{g L}^{-1}$ and $100 \mu\text{g L}^{-1}$) and their combination with MWCNTs (1 mg L^{-1}). Additional information to
1004 Figure 4a.

1005 **Table S4:** M-Values of DEGs in digestive gland of mussels exposed to increasing BaP concentrations
1006 ($5 \mu\text{g L}^{-1}$, $50 \mu\text{g L}^{-1}$ and $100 \mu\text{g L}^{-1}$) and their combination with MWCNTs (1 mg L^{-1}). Additional
1007 information to Figure 4b.

1008 **Figure S4:** Q-PCR confirmation of microarray data. Targets expressions have been analyzed by real-
1009 time PCR, using a 18S rRNA, Beta actin and Ribol27 as reference genes for data normalization. Data
1010 represent the mean of at least four independent experiments. Calculation of relative expression
1011 levels and statistics (pairwise randomization test, $p < 0.05$) were obtained using the REST software
1012 (Pfaffl *et al.* 2002). Experimental coefficient of variation (CV) was below 5% for all the investigated
1013 targets.

1014 **Figure S5.** (a,c,e) ESEM imaging and (b,d,f) corresponding point EDX spectroscopy analysis of whole
1015 mussel digestive gland tissues. The bright features (which comprise high atomic number elements) in
1016 the back scatter ESEM images are used to visually locate nanoscale species of interest. The EDX
1017 spectra are collected from these explicit locations and confirm the presence of Ca (b), Fe (d) and Pb
1018 (f) as expected environmental contaminants.

1019 **Figure S6.** (a,c,e) ESEM imaging and (b,d,f) corresponding point EDX spectroscopy analysis of whole
1020 mussel digestive gland tissues exposed to AuNP@MWCNT. The EDX spectra confirm the presence of
1021 Fe (b,d) and Pt (f) as environmental contaminants. No structures corresponding to labelled MWCNTs
1022 were detected either visually or spectroscopically in the whole tissue samples.

1023 **Figure S7.** (a,c,e) Dark field STEM imaging and (b,d,f) corresponding point EDX spectroscopy analysis
1024 of cross-sections of mussel digestive gland. The bright features (which comprise high atomic number
1025 elements) in the dark field STEM images are used to visually locate nanoscale species of interest. The
1026 EDX spectra are collected from these explicit locations and confirm the presence of Fe (b,f) and silica
1027 (d) as expected environmental contaminants.

1028 **Figure S8.** (a,c,e) Dark field STEM imaging and (b,d,f) corresponding point EDX spectroscopy analysis
1029 of cross-sections of mussel digestive gland exposed to AuNP@MWCNT. The EDX spectra confirm the
1030 presence of Fe (b), Ag (d) and silica (f) as expected environmental contaminants. No structures
1031 corresponding to labelled MWCNTs were detected either visually or spectroscopically in the cross-
1032 sections.